

# Robustness and Scalability Of Machine Learning for Imbalanced Clinical Data in Emergency and Critical Care

Yusuf Brima<sup>1,\*</sup> and Marcellin Atemkeng<sup>2,3</sup>

<sup>1</sup>Computer Vision Group, Institute of Cognitive Science, Osnabrück University, Osnabrueck, D-49090, Germany

<sup>2</sup>Department of Mathematics, Rhodes University, Grahamstown 6139, South Africa

<sup>3</sup>National Institute for Theoretical and Computational Sciences (NITheCS), Stellenbosch 7600, South Africa

\*ybrima@uos.de

## ABSTRACT

Emergency and intensive care environments require predictive models that are both accurate and computationally efficient, yet clinical (tabular) data in these settings are often severely imbalanced. Such skewness undermines model reliability, particularly for rare but clinically crucial outcomes, making robustness and scalability essential for real-world usage.

In this paper, we systematically evaluate the robustness and scalability of classical machine learning models on imbalanced tabular data from two large-scale clinical datasets (MIMIC-IV-ED and eICU). Class imbalance was quantified using complementary metrics, and we compared the performance of tree-based methods (Decision Tree, Random Forest, XGBoost), the state-of-the-art TabNet deep learning model, and a custom lightweight residual network (TabResNet). TabResNet was designed as a computationally efficient alternative to TabNet, replacing its complex attention mechanisms with a streamlined residual architecture to maintain representational capacity for real-time clinical use. All models were optimized via a Bayesian hyperparameter search and assessed on predictive performance (weighted F1-score), robustness to increasing imbalance, and computational scalability. Our objective was to provide evidence-based guidance for model selection in acute care settings. Our results, on seven clinically vital predictive tasks, show that tree-based methods, particularly XGBoost (an ensemble model family), consistently achieved the most stable performance across imbalance levels and scaled efficiently with sample size. Deep tabular models degraded more sharply under imbalance and incurred higher computational costs, while TabResNet provided a lighter alternative to TabNet but did not surpass ensemble benchmarks.

These findings indicate that in emergency and critical care, robustness to imbalance and computational scalability could outweigh architectural complexity. Tree-based ensemble methods currently offer the most practical and clinically feasible choice, equipping practitioners with a framework for selecting models suited to high-stakes, time-sensitive environments.

**Keywords:** Emergency Medicine, Intensive Care, Clinical Artificial Intelligence, Deep Learning, Machine Learning, Class Imbalance, Predictive Modeling, Electronic Health Record Data

## Introduction

In the emergency department (ED) and intensive care unit (ICU), clinicians often face many challenges of varying magnitude: high patient turnover, unpredictable workloads, and the need to make rapid decisions for life-threatening conditions<sup>1-3</sup>. In these high-stakes environments, minutes can determine survival, therefore, there is an impetus for decision support systems to provide both accurate and computationally efficient predictions<sup>4,5</sup>. Machine learning (ML), a subfield of Artificial Intelligence (AI), has emerged as a promising tool for enhancing clinical support under such constraints<sup>6-10</sup>, with applications ranging from diagnosis and prognosis to triage and disposition prediction.

Yet, healthcare data predominately present unique challenges. In addition to *high dimensionality* and *heterogeneity*, a defining issue is *class imbalance* where critical but rare outcomes (e.g., in-hospital death, cardiac arrest; or, in-clinical practice, septic shock) are represented by far fewer samples than their common counterparts. This can lead to biased models that perform well on majority classes but fail on minority ones, precisely where predictive accuracy could or would be most clinically valuable<sup>11,12</sup>.

These challenges have important implications for the choice of learning paradigm. While deep learning (DL), a subfield of ML, has transformed domains such as computer vision and natural language processing<sup>13-15</sup>, its application to tabular healthcare data under class imbalance remains limited<sup>16</sup>. DL architectures typically require large, balanced datasets to achieve optimal performance<sup>17,18</sup>. By contrast, traditional ML methods, particularly tree-based ensemble approaches such as random forests and gradient boosting (e.g., XGBoost), are widely used because of their robustness and interpretability in tabular data tasks<sup>19,20</sup>. Prior studies report mixed results: DL can outperform classical approaches with sufficient data and tuning<sup>21</sup>, but

tree-based models often prove more reliable on imbalanced healthcare datasets<sup>22,23</sup>.

To address these limitations, various strategies have been developed to mitigate the impact of imbalance, including resampling techniques such as Synthetic Minority Over-sampling TEchnique (SMOTE) and its derivatives<sup>24</sup>, cost-sensitive learning<sup>25</sup>, and specialized loss functions such as focal loss<sup>26,27</sup>. However, systematic evaluations of how these strategies interact with different *model families* (i.e., groups of models built on similar architectural principles such as feedforward neural networks, decision trees, random forests, or encoder-only Transformers, etc) under controlled imbalance remain underexplored. Moreover, state-of-the-art (SOTA) DL architectures for tabular data, such as TabNet<sup>28</sup>, are still not well characterized in emergency and critical care contexts, where time constraints and computational efficiency are in demand.

Against this backdrop, this study has three aims:

1. To empirically quantify class imbalance in ED/ICU data using multiple complementary metrics, and to assess how consistently these metrics capture imbalance phenomena across different datasets.
2. To systematically evaluate the effect of imbalance on the robustness, i.e., whether a model maintains reliable predictive performance when the minority class becomes increasingly underrepresented, of different model families.
3. To compare the computational efficiency of these model families as dataset size scales, clarifying the trade-offs that influence the feasibility of real-time or near real-time utilization in ED and ICU environments.

By addressing these aims, the study contributes (i) a framework for empirically assessing imbalance in large-scale clinical electronic health record (EHR) databases, (ii) systematic investigation on how imbalance affects the robustness of different model families, and (iii) an analysis of how computational requirements scale with data size, informing evidence-based guidance for model selection for this problem domain.

## Organization of the Paper

The remainder of this paper is organized as follows. The *Methods* section describes the databases, prediction tasks, model architectures and evaluation approaches utilized, as well as the procedures used to quantify and counteract class imbalance. The *Results* section presents our experimental outcomes. The *Discussion* section highlights our key findings and their implications for robustness and potential clinical deployment and adoption strategies. It also outlines avenues for further research. Finally, the *Conclusion* summarizes the main contributions of this work.

## Methods

In this section, we expound on the data utilized: their sources, characterization, preprocessing, and specific predictive tasks they tackle. Thereafter, we discuss the model architectures and their configurations used. Then, the optimization algorithm, including the training objectives, is discussed. After that, we explain both the imbalance quantification metrics and classification performance metrics. Finally, the experimental setup is stated.

### Healthcare Prediction Tasks and Datasets

To conduct this study, our goal was to use data that are clinically and contextually relevant to the problem in question. Therefore, the data sources were chosen because of their ideal fit for this purpose. In that regard, we describe these datasets below accordingly.

#### **MIMIC-IV-ED**

We used the *MIMIC-IV-ED* database (v2.2), which contains approximately 425,000 ED stays collected between 2011 and 2019 at Beth Israel Deaconess Medical Center in Boston, Massachusetts<sup>29</sup>. It is hosted on the PhysioNet platform<sup>30</sup> and includes detailed demographic information, triage measurements, periodic vital signs, medication administrations, and discharge diagnoses. Its rich clinical coverage makes it a suitable resource for evaluating ML models under realistic conditions such as class imbalance.

We defined three clinically relevant prediction tasks using this dataset. First, we aimed to predict the primary diagnosis at discharge, capturing the most pressing clinical issue during the ED stay. Second, we grouped diagnoses into three-character International Classification of Diseases (ICD 9 and 10) categories to assess model performance at a higher level of disease semantic abstraction, reducing label sparsity while retaining clinically meaningful distinctions. Third, we predicted ED disposition outcomes, including admission, discharge, transfer, or death, which reflect critical operational and patient safety considerations. These tasks span different levels of clinical granularity, enabling a comprehensive assessment of model robustness across diverse prediction scenarios.

To prepare the data for model training and evaluation, we applied systematic preprocessing and feature engineering steps, including handling of missing values, normalization of continuous variables, and encoding of categorical variables. We also

employed stratified sampling to ensure proportional representation of all target classes in the training, validation, and test splits. Additional details of the preprocessing workflow, feature construction, and dataset assembly are provided in Appendix .1.1.

### **eICU Collaborative Research Database (eICU-CRD)**

To complement the single-center MIMIC-IV-ED data and assess model robustness across multiple institutions, the eICU-CRD was utilized. It contains circa 200,000 ICU stays collected from multiple hospitals across the United States<sup>31</sup>. This multicenter dataset includes patient demographics, vital signs, laboratory measurements, clinical interventions, and outcomes, providing a broad context to evaluate the robustness of models across diverse hospital settings and patient demographics.

The prediction tasks closely mirrored those defined for MIMIC-IV-ED to enable cross-dataset comparisons of methods appropriately. These included mortality risk prediction, and patient disposition, such as ICU discharge, transfer, or death, etc. Maintaining comparable prediction tasks allows direct assessment of model performance under differing data distributions, class imbalances, and institutional practices.

Preprocessing and feature engineering followed the same principles applied to the prior dataset, including handling of missing values, normalization of continuous variables, and one-hot encoding of categorical variables. Stratified sampling preserved class distributions across training, validation, and test splits. Detailed descriptions of feature extraction, dataset assembly, and preprocessing for the eICU database are provided in Appendix .1.2.

## **Models Evaluated**

To assess the performance of the chosen ML algorithms, a range of methods was evaluated, spanning classical ML and SOTA DL approaches. This allowed for comparisons among interpretable tree-based models, modern attention-based architecture, and custom network design, with the goal of providing insight into their robustness and scalability under the problem being studied.

### **Traditional ML Models**

Classical ML algorithms remain widely applicable to structured data (used interchangeably with tabular data in this present work) because of their interpretability, robustness, and proven performance across diverse tasks. We chose three representative classical ML techniques to provide a strong basis for assessing whether more complex architectures yield tangible improvements, particularly under conditions of class imbalance. The first of these, the *decision tree* (DT) algorithm<sup>32</sup>, organizes data into a tree-like structure by *iteratively partitioning features at thresholds that maximize the reduction in impurity*, such as Gini impurity or entropy. Each internal node encodes a decision rule, and each leaf node corresponds to a predicted class.

Building on the simplicity of individual decision trees, the *random forest* (RF) algorithm<sup>33</sup> *constructs an ensemble of trees, each trained on a bootstrap sample of the data with a random subset of features*. Predictions are made by a *majority voting across the ensemble*, which reduces variance and improves generalizability. By aggregating multiple trees, RFs are reportedly robust toward noisy or imbalanced datasets.

To further extend this ensemble approach, the *XGBoost* algorithm<sup>34</sup> implements gradient boosting, sequentially constructing trees where *each new tree focuses on correcting the residual errors of its predecessors*. By optimizing a differentiable loss function with added regularization, XGBoost captures complex feature interactions while curtailing overfitting. We used XGBoost as a representative of gradient boosting methods; alternatives such as LightGBM<sup>35</sup> or CatBoost<sup>36</sup> primarily introduce engineering optimizations (e.g., histogram-based growth, leaf-wise splits, categorical handling), but comparative studies indicate that their robustness and scalability are broadly comparable to XGBoost<sup>37</sup>. As the aim of this work is to evaluate the behavior of model *families* under class imbalance and scaling, rather than to exhaustively benchmark every implementation, including additional boosting variants would add redundancy without altering the family-level outcomes.

Together, these classical methods establish a strong basis for predictive modeling in tabular clinical data. With this foundation in place, we next turned to SOTA DL architectures for structured data, allowing a more comprehensive assessment of how model complexity, attention mechanisms, and representation learning shape predictive performance, robustness, and scalability under class imbalance.

### **SOTA Deep Learning Models**

The primary DL model evaluated was **TabNet**<sup>38</sup>, an attention-based deep neural network tailored for tabular data. TabNet employs sequential attention to selectively focus on relevant features at each decision step, allowing the model to learn interpretable feature masks while capturing complex interactions. This balances predictive power with interpretability, addressing a key limitation of conventional counterparts when applied to structured datasets. Other advanced tabular architectures, such as **TabPFN**<sup>39</sup>, was also considered. However, owing to its substantial compute requirements, this class of models was excluded from the final evaluation, highlighting utilization constraints in real-world resource-limited settings even on a Quadro RTX 8000, 48 gigabytes graphics processing unit (GPU). By including TabNet, our study seeks to capture a representative SOTA learning approach while remaining mindful of computational feasibility in clinical settings.

**TabResNet**

Furthermore, we developed a custom deep neural network (TabResNet) specifically designed as a candidate deep model with reference to TabNet. Unlike TabNet, which relies on complex attention mechanisms that can be computationally prohibitive in real-time clinical settings, TabResNet prioritizes computational efficiency while maintaining representational capacity through strategic architectural choices.

The network architecture, as shown in Figure 1, was motivated by three key considerations for clinical usage: (1) fast training and inference for real-time or near real-time decision support, (2) stable training on imbalanced data, and (3) sufficient model capacity to capture complex feature interactions without overfitting on limited minority class samples.

To operationalize these design principles, the input processing layer was structured to combine linear transformation with batch normalization, Rectified Linear Unit (ReLU) activation, and dropout. This sequence addresses common challenges in clinical tabular data: batch normalization standardizes heterogeneous feature scales typical in EHR data, whereas dropout provides regularization crucial for small minority class samples.

The core of this architecture lies in the compact residual blocks (blocks 1–3, which are determined via hyperparameter optimization). Traditional deep networks often struggle with tabular data due to the limited benefit of depth compared with width. Our residual design enables stable gradient flow through deeper architectures while maintaining computational efficiency. Each block uses two linear transformations with intermediate normalization and activation, allowing the network to learn nonlinear feature combinations while the skip connection preserves the original feature information—which is particularly important when minority class patterns may be subtle.

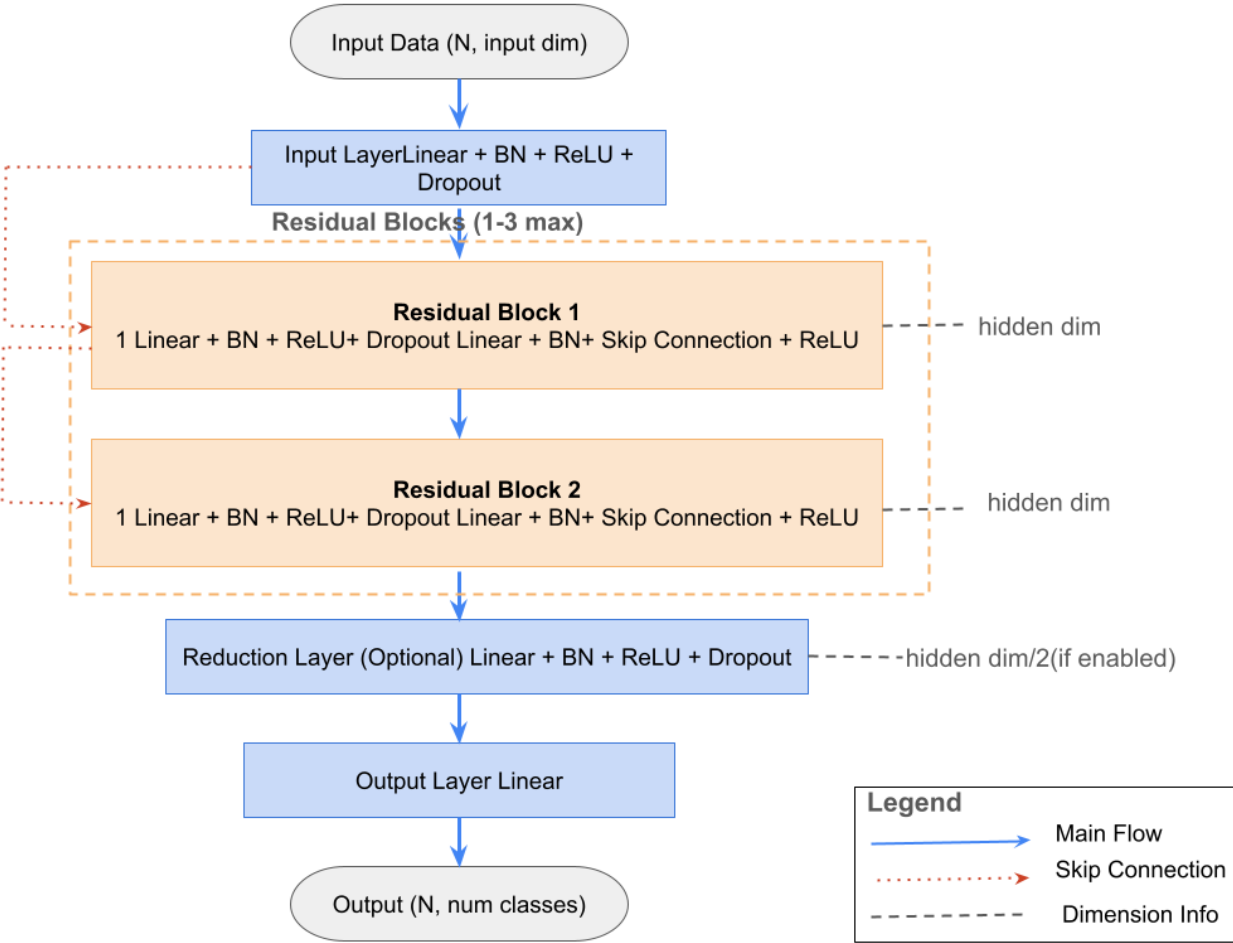


**Figure 1. Architecture of TabResNet.** Sequential structure of the network architecture for tabular data. The Input Layer (Linear + BatchNorm + ReLU + Dropout) is followed by 1–3 Compact Residual Blocks, each containing two Linear layers with Batch Norm, ReLU, Dropout, and a skip connection. An optional Reduction Layer precedes the Output Layer, which produces class predictions.



The optional reduction layer serves as a learned dimensionality reduction step, condensing representations before classification. This design choice was motivated by the often high-dimensional nature of clinical features, where dimensionality reduction can improve the generalizability of imbalanced datasets by focusing on the most discriminative feature combinations.

Compared with TabNet’s sequential attention mechanism, TabResNet achieves similar representational capacity with significantly reduced computational overhead (see Results), making it more suitable for deployment in resource-constrained clinical environments where inference speed is critical for patient care workflows.

The implementation leverages PyTorch for TabResNet and TabNet, whereas Scikit-learn is used for decision trees, random forests, and XGBoost. For final reporting, pre-set random seeds that followed experiment numbers were to ensure reproducibility across models.

## Class Imbalance Handling Strategies

We first introduced the notational framework used throughout this section, which subsequently allowed us to define precisely how imbalance is quantified and addressed.

Throughout, we write scalars in italics (e.g.,  $n, d, K$ ), vectors in bold lowercase (e.g.,  $\mathbf{x}, \mathbf{z}$ ), and matrices in bold uppercase (e.g.,  $\mathbf{X} \in \mathbb{R}^{N \times d}$ ). Sets and spaces are denoted in calligraphic font (e.g.,  $\mathcal{D}, \mathcal{X}, \mathcal{Y}, \mathcal{Z}$ ), while functions and mappings are written in standard math operator style (e.g.,  $f, \sigma, \text{softmax}$ ). In particular, we use  $\mathbf{x}_i$  to denote an *individual input vector* and  $\mathbf{X}$  for the *design matrix* containing all samples stacked row-wise. This convention ensures a clear distinction between observed data  $(\mathbf{x}_i, y_i)$ , latent representations  $\mathbf{z}_i$ , predictions  $\hat{y}_i$ , and the mappings that connect them.

### Dataset and Input Space

Let a dataset be denoted as  $\mathcal{D} := \{(\mathbf{x}_i, y_i)\}_{i=1}^N$  where  $N \in \mathbb{N}$  is the total number of samples. Each input  $\mathbf{x}_i \in \mathcal{X}$  belongs to the feature space  $\mathcal{X} \subseteq \mathbb{R}^d$  with  $d$  the dimensionality.

### Label Space

Each label  $y_i \in \mathcal{Y}$ , where  $\mathcal{Y} = \{1, 2, \dots, K\}$  is a discrete variable representing one of  $K$  possible classes. For multi-class classification,  $y_i$  may be equivalently represented as a one-hot vector in  $\{0, 1\}^K$ . We denote the vector of all labels as  $\mathbf{y} = (y_1, \dots, y_N)^\top$ .

### Latent (Logit) Space

The model, in a general sense, is a function  $f : \mathcal{X} \rightarrow \mathcal{Z}$  mapping feature vectors to latent representations. For each input  $\mathbf{x}_i$ , it produces logits  $\mathbf{z}_i \in \mathcal{Z}$ , where  $\mathcal{Z} \subseteq \mathbb{R}^K$  in the multi-class case and  $\mathcal{Z} \subseteq \mathbb{R}$  for binary classification. We denote vectors of logits as  $\mathbf{z}_i \in \mathbb{R}^K$  and the stacked matrix as  $\mathbf{Z} \in \mathbb{R}^{N \times K}$ . These logits are transformed into probabilities through activation functions:

$$\begin{aligned} \sigma : \mathbb{R} &\rightarrow [0, 1], & (\text{sigmoid for binary tasks}), \\ \text{softmax} : \mathbb{R}^K &\rightarrow [0, 1]^K, & (\text{softmax for multi-class tasks}). \end{aligned}$$

The predicted label is then obtained as:

$$\hat{y}_i = \arg \max_{k \in K} \hat{y}_{i,k}.$$

We denote the probability vector for sample  $i$  as  $\hat{\mathbf{y}}_i \in [0, 1]^K$  and the full prediction matrix as  $\hat{\mathbf{Y}} \in [0, 1]^{N \times K}$ .

With this formalization in place, we now describe strategies to address class imbalance during training. We focused on approaches that can be applied consistently across both classical ML algorithms and deep architectures. While alternative methods such as focal loss<sup>26</sup> have been proposed specifically for neural networks to emphasize hard-to-classify examples, they are less straightforward in tree-based models or other classical algorithms. To ensure comparability across model families, we implemented three complementary weighting strategies derived directly from the label distribution.

The first, **Inverse Frequency** which is widely adopted, assigns a weight to each class inversely proportional to its number of samples in that class. For class  $k$ , the weight is computed as:

$$w_k = \frac{N}{K N_k}, \tag{1}$$

where  $N$  is the total number of training samples,  $K$  the number of classes, and  $N_k$  the number of samples in class  $k$ . This ensures that minority classes contribute more during training.

The second strategy, **Effective Number of Samples**<sup>40</sup>, accounts for the diminishing benefit of additional samples from frequent classes. Let  $\beta \in [0, 1]$  be a smoothing factor. The effective number of samples for class  $k$  is:

$$N_k^{\text{eff}} = \frac{1 - \beta^{N_k}}{1 - \beta},$$

with the corresponding normalized weight:

$$w_k = \frac{1}{N_k^{\text{eff}}} \frac{\sum_{j=1}^K N_j^{\text{eff}}}{K}.$$

This reduces the dominance of majority classes while avoiding excessively large weights for rare ones.

The third approach, **Median Frequency Balancing**, scales the weight of each class by the ratio of the median class frequency to the class's frequency:

$$w_k = \frac{\text{median}(f_1, \dots, f_K)}{f_k}, \quad f_k = \frac{N_k}{N},$$

where  $f_k$  is the relative frequency of class  $k$ . This method balances contributions without allowing rare classes to dominate excessively.

These computed weights  $\{w_k\}_{k=1}^K$  are incorporated directly into the loss functions for both binary and multi-class tasks, ensuring that minority classes exert proportional influence during optimization. This is supposed to improve detection of rare but clinically significant outcomes while maintaining training stability.

### Class Imbalance Quantification

To evaluate model robustness systematically, we filtered the composition of each dataset to create controlled levels of class imbalance. This was achieved by varying the minimum number of samples required for each class within that dataset. Lower thresholds retain rarer classes, producing training and evaluation candidate dataset with pronounced imbalance (i.e., skewed distributions), whereas higher thresholds favor more common classes, resulting in a nearly more uniform distribution.

To assess these effects, we quantified the degree of imbalance via three complementary metrics, each capturing a property of class representation.

#### Coefficient of Variation of Class Frequency (CVCF)

The first metric, the CVCF, measures the relative variability in class *frequencies*, highlighting whether some classes dominate the dataset.

For each class  $k$ , the relative frequency is calculated as:

$$f_k = \frac{N_k}{N}. \quad (2)$$

Given these frequencies  $\{f_k\}_{k=1}^K$ , the CVCF is defined as:

$$\begin{aligned} \bar{f} &= \frac{1}{K} \sum_{k=1}^K f_k && \text{(mean class frequency),} \\ \sigma_f &= \sqrt{\frac{1}{K} \sum_{k=1}^K (f_k - \bar{f})^2} && \text{(standard deviation of class frequencies),} \\ \text{CVCF} &= \frac{\sigma_f}{\bar{f}} && \text{(coefficient of variation).} \end{aligned} \quad (3)$$

A higher CVCF signals pronounced imbalance, with certain classes disproportionately represented, whereas a lower CVCF reflects more uniform class distributions.

#### Imbalance Ratio (IR)

Complementing the CVCF, the IR captures the disparity between the most and least represented classes. Let  $\{N_k\}_{k=1}^K$  denote class counts:

$$\text{IR} = \frac{\max_k N_k}{\min_k N_k}, \quad \min_k N_k > 0. \quad (4)$$

An IR of 1 indicates perfectly balanced classes, while higher values correspond to increasingly skewed distributions. Unlike CVCF, which accounts for all class frequencies, IR focuses specifically on the extremes of the distribution.

### Normalized Entropy of Class Distribution (NECD)

While CVCF captures variability across all classes and IR emphasizes extremes, both are inherently scale-free statistics: CVCF is a ratio of dispersion to mean, and IR is a ratio of maximum to minimum class counts. Their values are directly comparable across problems with different numbers of classes. Entropy provides a complementary perspective by quantifying the uncertainty of predicting a random class label, reaching its maximum under a uniform distribution and decreasing as the distribution becomes skewed. Unlike CVCF and IR, however, the raw value of entropy depends on the number of classes  $K$ , which makes direct comparisons across tasks misleading. To address this, we normalize entropy by its maximum possible value, ensuring that the measure consistently reflects class balance irrespective of  $K$ .

Using the relative frequencies  $\{f_k\}_{k=1}^K$  defined in Equation 2, the Shannon entropy is

$$H = - \sum_{k=1}^K f_k \log f_k, \quad (5)$$

with  $f_k \log f_k = 0$  when  $f_k = 0$ . The maximum entropy is

$$H_{\max} = \log(K), \quad (6)$$

corresponding to a perfectly uniform distribution. The normalized entropy is then

$$\text{NECD} = \frac{H}{H_{\max}} = \frac{-\sum_{k=1}^K f_k \log f_k}{\log(K)}. \quad (7)$$

NECD ranges from 0 (complete imbalance) to 1 (perfect balance), with intermediate values reflecting partial uniformity.

Together with CVCF and IR, it provides a complementary measure for generating datasets with controlled imbalance and analyzing their impact on model performance.

### Model Predictive Performance Evaluation

We evaluated the predictive performance of all models using two complementary metrics: overall accuracy and the weighted F1 score. Accuracy measures the fraction of correct predictions across all samples as shown in equation 8, providing a straightforward assessment of overall model correctness. However, in datasets with class imbalance, accuracy can give a distorted view of performance because *it can be dominated by the majority classes*, masking poor performance on clinically important minority classes.

For a dataset with  $N$  samples, we denote the ground-truth labels as  $y_i$  and the model's predicted class as  $\hat{y}_i$ . Overall accuracy is computed as:

$$\text{Accuracy} = \frac{1}{N} \sum_{i=1}^N \mathbb{1}\{y_i = \hat{y}_i\}, \quad (8)$$

where  $\mathbb{1}\{\cdot\}$  is the indicator function, equal to 1 if the condition inside is true and 0 otherwise.

The F1 score on the other hand provides a balanced measure of precision and recall for each class. For a given class  $k \in \{1, \dots, K\}$ , we define:

$$\text{Precision}_k = \frac{\text{TP}_k}{\text{TP}_k + \text{FP}_k}, \quad \text{Recall}_k = \frac{\text{TP}_k}{\text{TP}_k + \text{FN}_k},$$

where  $\text{TP}_k$ ,  $\text{FP}_k$ , and  $\text{FN}_k$  denote the number of true positives, false positives, and false negatives for class  $k$ , respectively.

The F1 score for class  $k$  is then:

$$\text{F1}_k = \frac{2 \cdot \text{Precision}_k \cdot \text{Recall}_k}{\text{Precision}_k + \text{Recall}_k}. \quad (9)$$

For multi-class tasks, we report the (weighted) F1, defined as the mean of  $\text{F1}_k$  across all  $K$  classes:

$$\text{F1} = \frac{1}{K} \sum_{k=1}^K \text{F1}_k.$$

By reporting both metrics, our goal is to ensure a more comprehensive and reliable assessment of predictive performance, capturing both the overall correctness and the model's ability to correctly identify minority classes.

In this formulation,  $y_i$  comes directly from the dataset, and  $\hat{y}_i$  is obtained from the model outputs. For binary classification, the model produces a single logit  $z_i \in \mathbb{R}$ , which is transformed into a probability through the sigmoid function

$$\hat{y}_i = \sigma(z_i) = \frac{1}{1 + e^{-z_i}}.$$

For multi-class classification, the model outputs a logit vector  $\mathbf{z}_i \in \mathbb{R}^K$ , which is converted to a probability distribution by the softmax function:

$$\text{softmax}(\mathbf{z}_i)_k = \frac{e^{z_{i,k}}}{\sum_{j=1}^K e^{z_{i,j}}}, \quad k = 1, \dots, K.$$

The predicted label  $\hat{y}_i$  is then obtained by selecting the most probable class:

$$\hat{y}_i = \arg \max_{k \in \{1, \dots, K\}} \hat{y}_{i,k}.$$

These outputs are the direct result of training the models to minimize task-specific loss functions, as described below.

### Objective Functions

To generate the predictions used in the metrics above, we optimized models by minimizing standard cross-entropy loss functions, adapting them to the type of classification task and explicitly incorporating class weights to address imbalance.

#### Binary Cross-Entropy For Binary Classification Tasks

In binary classification tasks, each sample belongs to one of two classes (e.g., ED disposition: admitted versus discharged). For each sample  $i$ , the ground-truth label is  $y_i \in \{0, 1\}$ , and the model produces a predicted probability  $\hat{y}_i \in [0, 1]$  for the positive class through a sigmoid output layer. To correct for imbalance, we applied class-dependent weights  $w_{y_i}$  (see Class Imbalance Handling Strategies). The weighted binary cross-entropy (BCE) loss is thus:

$$\ell_{\text{BCE}}(y, \hat{y}) = -\frac{1}{N} \sum_{i=1}^N w_{y_i} [y_i \log(\hat{y}_i) + (1 - y_i) \log(1 - \hat{y}_i)].$$

#### Categorical Cross-Entropy For Multi-Class Classification Tasks

In multi-class classification, each sample belongs to one of  $K$  classes (e.g., primary diagnosis at discharge). The ground-truth label for sample  $i$  is encoded as a one-hot vector  $y_{i,k}$ , and the model outputs logits that are passed to a softmax layer to produce class probabilities  $\hat{y}_{i,k}$ , ensuring the probabilities sum to 1 in accordance with the law of total probability. As in the binary case, we introduced class-specific weights  $w_k$  to mitigate imbalance, with minority classes assigned larger values. The weighted categorical cross-entropy (CCE) loss is therefore:

$$\ell_{\text{CCE}}(y, \hat{y}) = -\frac{1}{N} \sum_{i=1}^N \sum_{k=1}^K w_k y_{i,k} \log(\hat{y}_{i,k}).$$

In both cases, as it is a *standard supervised learning setup*, the loss  $\ell(y, \hat{y})$  explicitly depends on the ground-truth labels  $y$  provided by the dataset, the predicted probabilities  $\hat{y}$  produced by the model, and the class weights  $\{w_k\}$  derived using a class weighting technique. Incorporating these class weights modifies the effective empirical distribution seen by the optimizer: samples from minority classes are given proportionally greater influence, while those from majority classes are down-weighted. This adjustment reshapes the loss landscape by amplifying gradients associated with underrepresented classes and dampening those from dominant ones, thereby reducing the bias toward majority classes.

From a statistical learning standpoint, this weighting can be viewed through the lenses of *risk minimization*. The theoretical goal of supervised learning is to minimize the *expected risk*:

$$R(h) = \mathbb{E}_{(\mathbf{x}, y) \sim P} [\ell(y, h(\mathbf{x}))] = \int \ell(y, h(\mathbf{x})) dP(\mathbf{x}, y),$$

where  $P$  is the true but unknown data-generating distribution. In practice, training minimizes the *empirical risk*:

$$\hat{R}(h) = \mathbb{E}_{(\mathbf{x}, y) \sim \hat{P}} [\ell(y, h(\mathbf{x}))] = \frac{1}{N} \sum_{i=1}^N \ell(y_i, h(\mathbf{x}_i)),$$

which approximates  $R(h)$  under the empirical distribution  $\hat{P}$  of the observed dataset. In imbalanced settings, however, this empirical distribution does not faithfully represent  $P$  or the clinically meaningful importance of classes: majority classes dominate, while minority classes are underrepresented.

Class weights provide a principled mechanism to re-weight  $\hat{R}(h)$  so that it better approximates a desired risk  $R_Q(h)$  under some target distribution  $Q$ . This re-weighting can be *interpreted as analogous to importance sampling*, since the weights  $w_k$  adjust the contribution of each class to better reflect  $Q$  (e.g., a balanced distribution). In effect, the optimizer no longer minimizes the risk under the raw empirical distribution but under a re-weighted surrogate distribution that emphasizes rare yet clinically critical outcomes. While this promotes more equitable learning across classes, excessively large weights can also inflate gradient variance for minority classes, which may destabilize training—underscoring the need for carefully designed weighting strategies.

Intuitively, this process can be viewed as a *transport of distributions*: the observed empirical distribution  $\hat{P}$  is skewed toward majority classes, while the desired target distribution  $Q$  places greater or proportionate mass on minority or clinically critical classes. Class weights  $\{w_k\}$  act as the transport coefficients, redistributing probability mass so that the weighted empirical risk  $\hat{R}_w(h)$  becomes a closer surrogate to the theoretical risk  $R_Q(h)$ . From this perspective, class weighting not only corrects for dataset imbalance but also realigns the optimization objective with the distribution one wishes to learn under, bridging the gap between observed data and theoretical desiderata.

## Hyperparameter Optimization

To ensure optimal and fair comparisons of model performance, systematic hyperparameter optimization was essential. All the models were tuned via Optuna<sup>41</sup>, a SOTA Bayesian optimization framework that employs tree-structured Parzen estimator (TPE) sampling to explore hyperparameter spaces efficiently. This approach adaptively focuses computational resources on promising regions on the basis of previous trials, ensuring comprehensive yet efficient optimization across all model architectures.

For each model, we defined comprehensive search spaces covering key hyperparameters that significantly impact performance, as detailed in Appendix .1.5. The optimization process consisted of 100 trials per model-dataset combination, with each trial evaluated via 5-fold cross-validation to ensure robust hyperparameter selection. The objective function was the F1 score on the validation set, which was aligned with our primary evaluation metric. Early stopping was implemented for DL models to prevent overfitting and reduce computational overhead.

Following hyperparameter optimization, the best configuration for each model family was used to train the final models. These optimized models were then evaluated on the held-out test set to generate the results reported in this study. This systematic approach ensures that performance differences between models reflect their inherent capabilities rather than suboptimal hyperparameter choices.

## Experimental Setup and Evaluation

All datasets were split into stratified train, validation, and test partitions (60–20–20%) to preserve class distributions. Model performance was primarily assessed using the weighted F1-Score, which is well-suited for imbalanced classification tasks. To evaluate computational efficiency, training times were recorded. Each experiment was repeated for 10 runs with different random seeds. Results are reported as mean  $\pm$  standard deviation, ensuring statistical robustness. All experiments were conducted independently on the MIMIC-IV-ED and eICU datasets.

## Results

Here, we present the empirical findings. These results are structured to first get a sense of the overall class distributions and an assessment of the degree of correlation among the imbalance metrics, followed by an analysis of predictive performance across models with respect to specific dataset and tasks, and finally, a comparison of training efficiency and scalability. Where appropriate, extended figures and analyses are provided in the Appendix to complement our main results.

### Correlation of Class Imbalance Metrics

The distributions of the targets across both datasets are presented in Figure 2. The MIMIC-IV-ED dataset exhibits a strong imbalance across all three prediction targets, most especially for diagnosis and ICD groupings, whereas the eICU dataset showed similar skewed patterns for mortality risk, length of stay, severity, discharge disposition, and resource utilization. To quantify imbalance, we computed the CVCF, IR, and NECD across weighting strategies per prediction target. Correlation analyses of these metrics are shown in Figure 3 for *MIMIC-IV-ED* and Figure 11 for eICU (see Appendix .3.1). Consistent associations were observed across metrics and prediction tasks, confirming that the selected measures capture complementary but related aspects of class distribution skew. As expected, NECD showed strong inverse correlation with IR and CVCF, highlighting its ability to provide an interpretable, bounded measure of class balance.



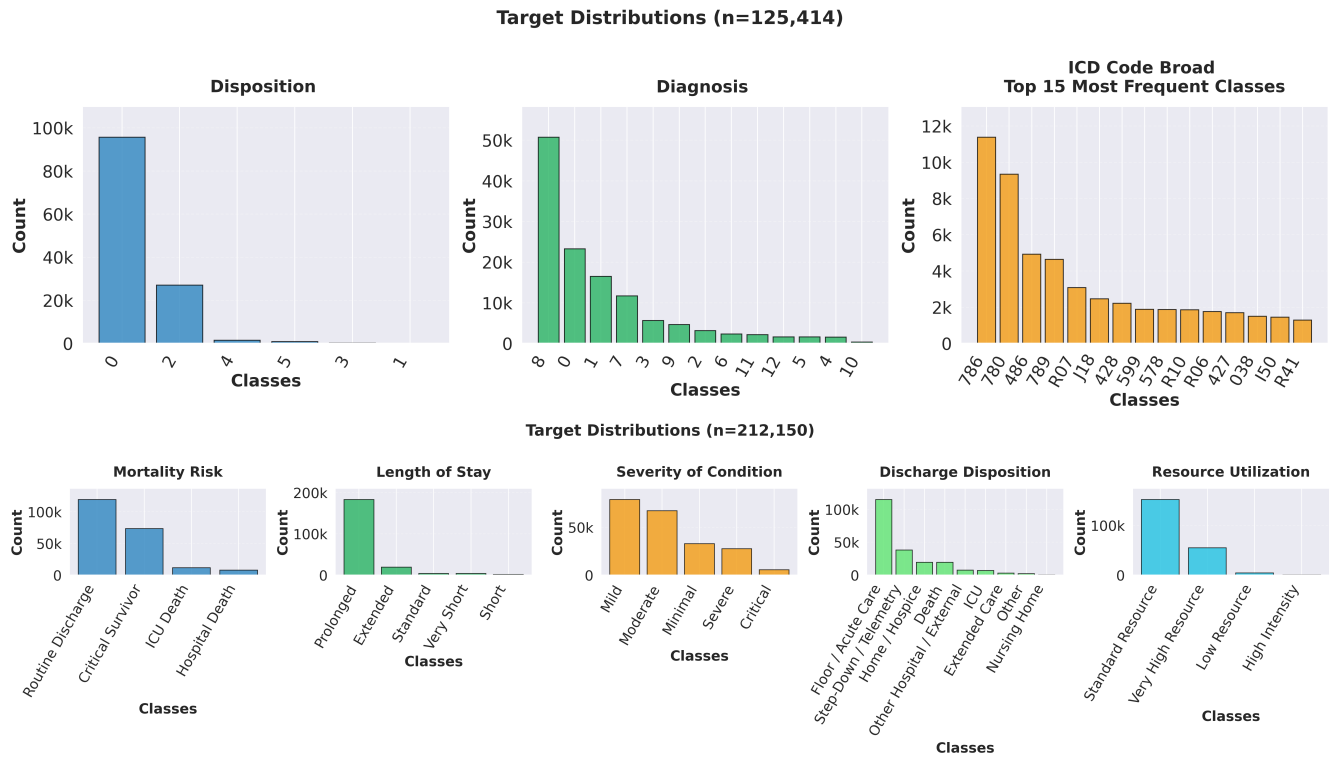


**Figure 2. Class distribution of target outcomes.** Class distribution of target variables in the MIMIC-IV-ED (top row) and eICU (bottom row) datasets. The histograms illustrate the frequency of samples across various clinical prediction tasks.

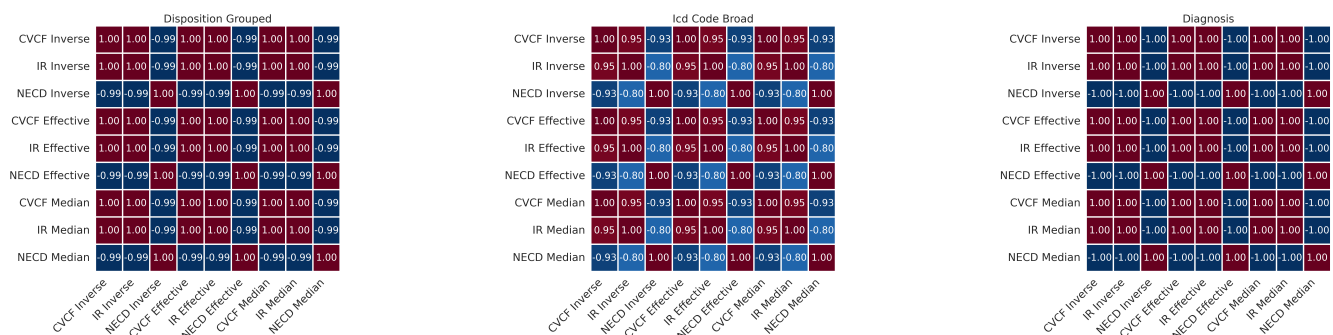


**Figure 3. Correlation of class imbalance metrics (MIMIC-IV-ED).** Correlation heatmaps of class imbalance metrics for different prediction tasks on the MIMIC-IV-ED dataset. Pairwise correlations are shown between the CVCF, IR, and NECD metrics across weighting strategies (inverse, effective, median) for three prediction tasks.

Notably, the strength of association among imbalance metrics varied by prediction target. For outcomes with only a few categories (i.e., low-cardinality settings, where the number of possible outcomes is small, such as ED disposition in MIMIC-IV-ED), all three measures were highly correlated. This is because when there are only a handful of outcomes, skew in the class distribution could be simple and, if pronounced, IR, CVCF, and NECD all capture essentially the same imbalance pattern.

By contrast, for outcomes with many possible categories (i.e., high-cardinality settings, such as diagnosis prediction, where many categories exist), correlations between CVCF and the other two measures were somewhat weaker. This reflects its greater sensitivity to distributional spread across many moderately rare classes, whereas IR emphasizes extremes (largest vs. smallest class) and NECD captures overall bounded distributional uncertainty. Nevertheless, CVCF remained directionally consistent with the other two metrics, complementing them. IR and NECD tended to remain more tightly coupled, whereas CVCF added nuance by highlighting variability across a wider range of classes. This pattern was also observed in the eICU dataset (Appendix .3.1), indicating that the behavior of CVCF in high-cardinality tasks is reproducible across datasets.

### Classifier Performance Comparison

We evaluated classifier performance in terms of the weighted F1 across increasing levels of imbalance. Figures 4–6 present the results for primary diagnosis, ICD grouping, and discharge disposition prediction in the MIMIC-IV-ED dataset, and Appendix .3.2 Figures 13–17 reports the corresponding eICU results. Weighted F1 scores, unsurprisingly, declined as imbalance increased, but the extent of degradation varied by task and classifier type.

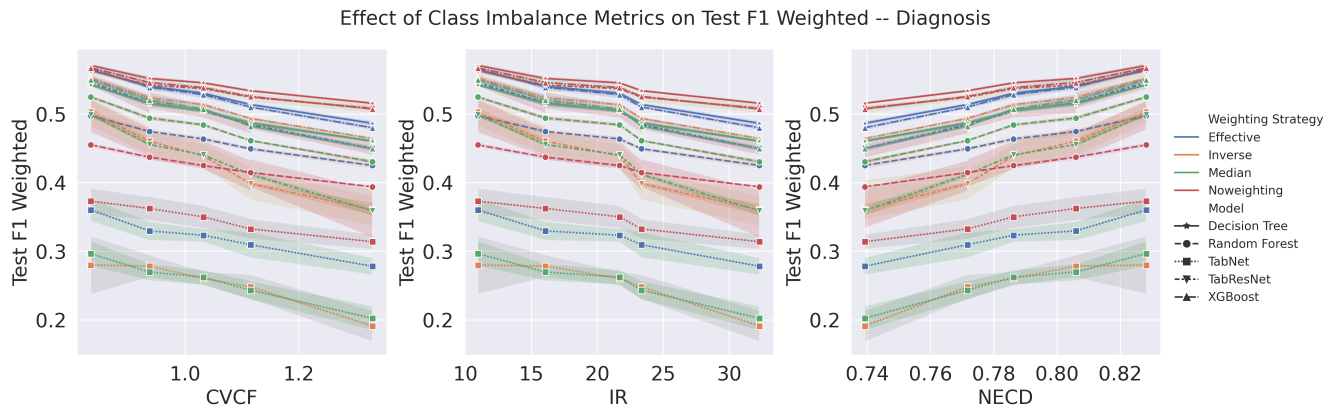


**Figure 4. Effect of class imbalance on discharge diagnosis.** Weighted F1 performance across varying levels of class imbalance for primary diagnosis prediction. The performance curves for 20 classifiers are shown, with the weighted F1 value decreasing as the imbalance severity increases.

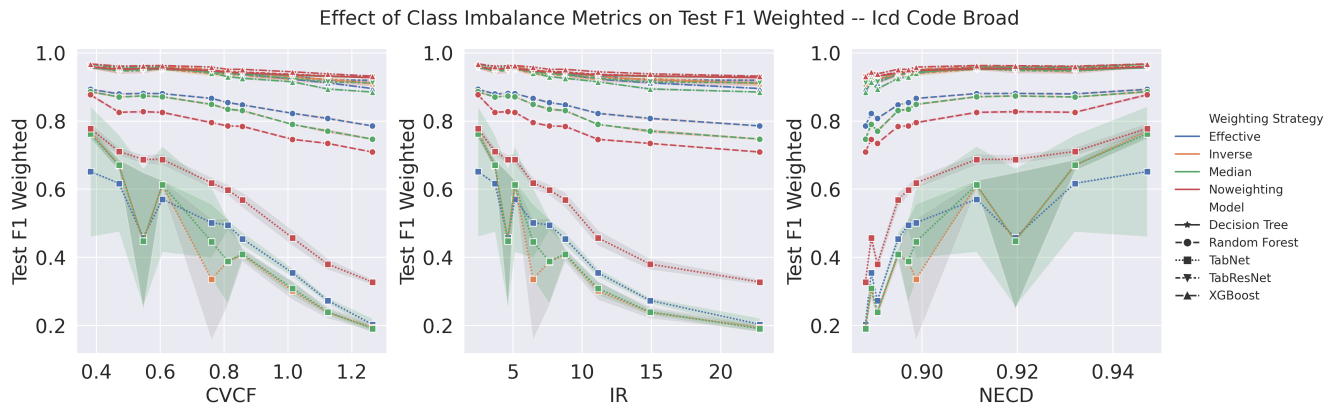


**Figure 5. Effect of class imbalance on ICD Code prediction.** Weighted F1 performance across varying levels of class imbalance for ICD code group prediction. Compared with fine-grained diagnosis prediction, grouped ICD categories reduce label sparsity, and classifiers generally maintain greater stability.

Effect of Class Imbalance Metrics on Test F1 Weighted -- Disposition Grouped

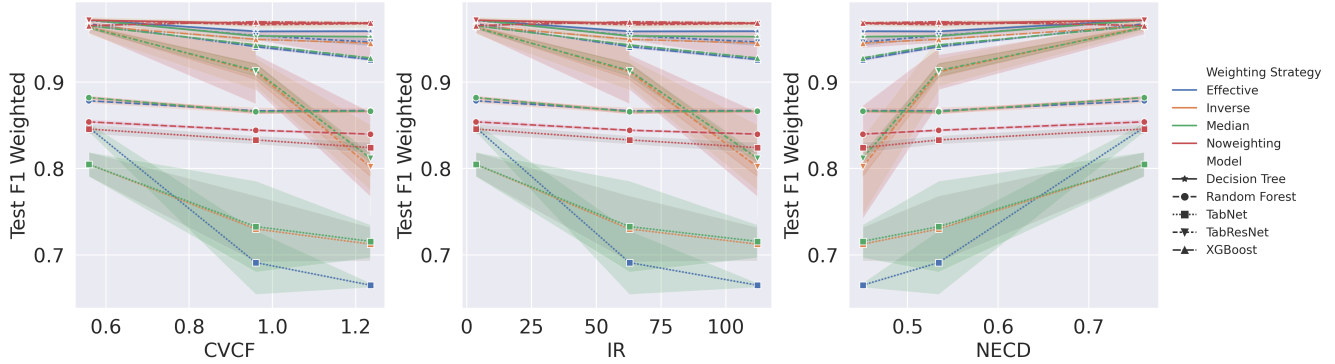


**Figure 6. Effect of class imbalance on disposition prediction.** Weighted F1 performance across varying levels of class imbalance for patient disposition prediction. The prediction of discharge outcomes shows moderate robustness to imbalance, with tree-based ensembles consistently outperforming deep learning models.

Performance decreased most sharply for fine-grained diagnosis prediction, where the large number of rare outcome categories amplified the effects of skewness. ICD Code prediction target showed more stable performance because aggregating codes reduced label sparsity to a certain extent. Disposition prediction exhibited intermediate sensitivity: the outcome space contained only a few categories, yet uneven class frequencies still led to measurable decline.

Across all tasks, degradation patterns were consistent across the three imbalance metrics. Specifically, increases in IR and CVCF, or decreases in NECD (approaching 0 from its maximum of 1 under perfect balance), were associated with monotonic declines in weighted F1. In high-cardinality tasks such as diagnosis prediction, curves based on CVCF were directionally aligned with those from IR and NECD but appeared slightly more variable, reflecting CVCF's heightened sensitivity to distributional spread across moderately rare classes. In contrast, for low-cardinality outcomes such as disposition, all three metrics produced nearly indistinguishable degradation curves. Together, these results confirm that while the metrics emphasize imbalance from different perspectives, they ultimately converge on the same conclusion: predictive performance declines predictably as imbalance severity increases.

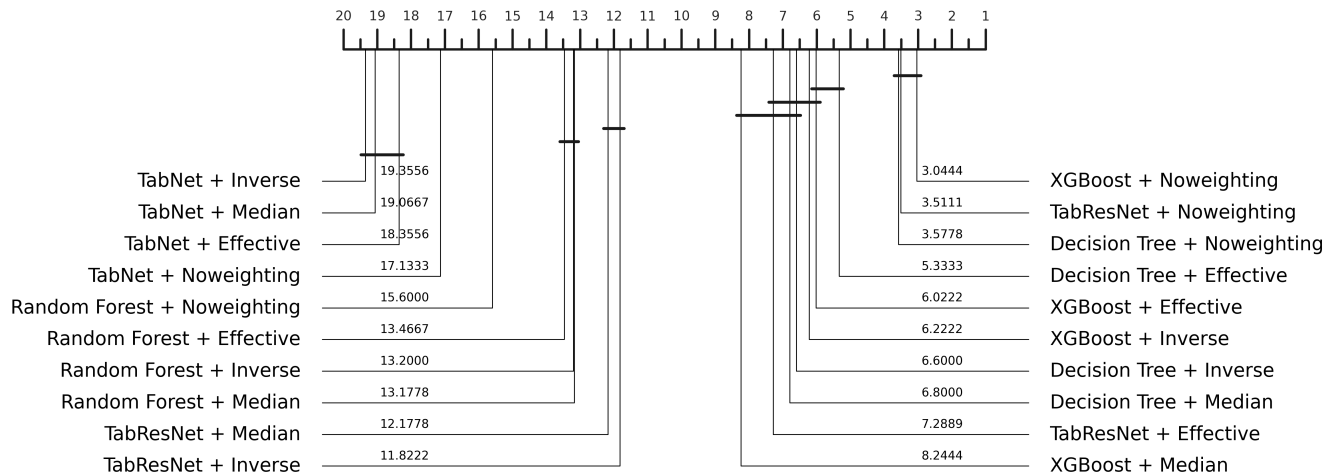


**Figure 7. Critical difference analysis of classifier performance.** This shows the average ranks of 20 classifiers on the basis of their weighted F1 performance across experimental blocks. Lower ranks indicate better predictive performance. The classifiers connected by a horizontal bar are not significantly different from each other according to Wilcoxon signed-rank tests with Holm correction.

To assess whether these performance differences across classifiers were statistically significant, we conducted a Friedman test, which confirmed significant differences in predictive performance among classifiers for both datasets (*MIMIC-IV-ED*:

$\chi^2(19, N = 45) = 737.91, p = 3.30 \times 10^{-144}$ ; eICU:  $\chi^2(19, N = 40) = 506.85, p = 2.04 \times 10^{-95}$ ). Here the 19 degrees of freedom correspond to the  $k - 1$  comparisons among the 20 classifiers (5 model families  $\times$  4 weighting strategies). The number of blocks  $N$  reflects the distinct prediction tasks crossed with training sample sizes (MIMIC-IV-ED: 3 targets  $\times$  15 filter sizes = 45 blocks; eICU: 5 targets  $\times$  8 filter sizes = 40 blocks), with performance values averaged across 10 experimental runs within each block. Post-hoc pairwise comparisons using Wilcoxon signed-rank tests with Holm correction are summarized in Figure 7 for MIMIC-IV-ED and Figure 12 for eICU (Appendix .3.2).

On the MIMIC-IV-ED dataset, XGBoost variants consistently achieved the lowest ranks, followed by Decision Tree and TabResNet, while TabNet and Random Forest variants exhibited higher ranks. On the eICU dataset, XGBoost variants again dominated in performance, with Random Forest and Decision Tree following, whereas TabResNet and TabNet generally occupied higher ranks.

Across both datasets, we further observed that weighting strategies based on the effective number of samples were never outperformed by alternative schemes (inverse or median frequency weighting), and often matched or exceeded their performance. This suggests that effective weighting provides a robust baseline for mitigating imbalance, regardless of model family or dataset.

Having established these performance differences, we next examine the efficiency of model training as dataset size and imbalance scale.

### Training Time Comparison

To this end, training efficiency was compared across models via both rank-based comparisons and scaling curves. We evaluated the training times of the 20 classifiers across their respective experimental blocks, each corresponding to a unique combination of a target variable and a training set size. A Friedman test revealed a statistically significant difference in training times among classifiers (MIMIC-IV-ED:  $\chi^2(19, N = 45) = 321.66, p = 7.12 \times 10^{-57}$ ; eICU:  $\chi^2(19, N = 40) = 244.54, p = 3.93 \times 10^{-41}$ ). Post hoc pairwise comparisons via Wilcoxon signed-rank tests with Holm correction (Figure 8 for MIMIC-IV-ED and Figure 18 for eICU) revealed that classical ML variants achieved the lowest average ranks (fastest training times), followed by random forest and TabResNet variants, whereas TabNet variants consistently required the longest times primarily due to its utilization of *iterative attention-based feature selection and layer-wise sequential processing*. The results on the eICU dataset mirrored this pattern, with traditional ML again achieving the lowest ranks, followed by TabResNet and random forest, and TabNet variants exhibiting the highest training times (Appendix .3.3). Extended analyses of training time scaling with dataset size are presented in Figures 10 (Appendix .2.1) and 19 (Appendix .3.4).

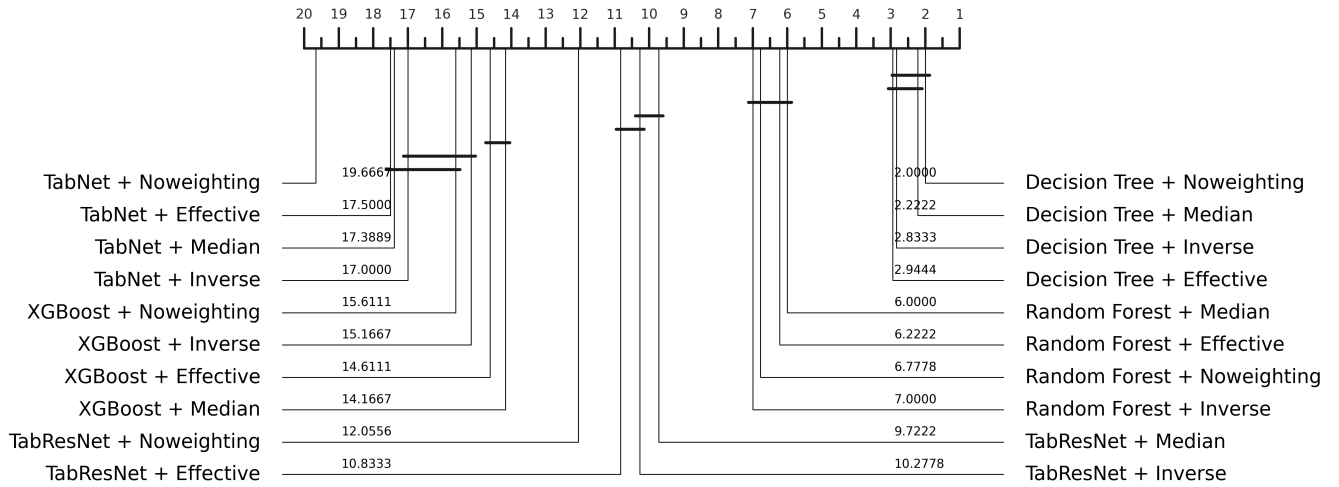


**Figure 8. Critical difference analysis of classifier training times.** This shows the average ranks of 20 classifiers based on their training times across 15 experimental blocks (each block is a unique combination of target variable and training set size). Lower ranks indicate faster training. Classifiers connected by a horizontal bar are not significantly different from each other according to Wilcoxon signed-rank tests with Holm correction.

### Discussion

In this section, we interpret our main findings. We discuss three main themes: (i) the associative relationship between imbalance metrics and performance degradation, (ii) the computational scaling behavior of different architectures, and (iii) the relative

advantages of ensemble methods compared with deep tabular models. We then consider broader implications, including cross-institutional robustness and generalization, clinical deployment, and equity considerations.

### Quantifiable Performance Degradation Under Imbalance

Our evaluation revealed consistent, often monotonic relationships between imbalance severity and performance degradation across model types and prediction targets of varying complexity. Critically, we found that IR, NECD, and CVCF exhibited strong correlations with one another across all targets and datasets, suggesting these metrics capture fundamentally related aspects of class distribution, albeit through different mathematical formalizations.

IR emphasizes the extremes by quantifying the ratio between the most and least frequent classes, NECD captures overall distributional uncertainty across all classes on a bounded  $[0, 1]$  scale (with 1 indicating perfect balance and 0 complete imbalance), and CVCF measures the relative dispersion of class frequencies, emphasizing variability in the distribution. Despite their distinct computational approaches, all three metrics proved monotonically related to performance degradation: as imbalance severity increased (reflected by higher IR and CVCF or lower NECD), model performance systematically declined. The strong correlations between these metrics, particularly between IR and NECD confirm they are measuring similar underlying phenomenon of class skewness from complementary mathematical perspectives. CVCF showed similarly strong correlations, though with slightly weaker associations in extremely high-cardinality targets where its sensitivity to moderate class frequency variations becomes more pronounced relative to the extreme-focused IR.

Importantly, this convergence across metrics strengthens rather than diminishes their practical utility. The fact that three derived imbalance measures consistently associated similar performance degradation patterns provides robust evidence that class distribution imbalance is a quantifiable, predictable challenge. This raises a practically important question: if dataset imbalance can be reliably quantified using any of these metrics, can model performance under imbalance be anticipated in advance without exhaustive experimentation?

Our results suggest some light on that. The monotonic, predictable relationships between imbalance metrics and performance degradation indicate that simple, computationally inexpensive imbalance scores can serve as reliable predictors of expected model robustness. While the three metrics are highly correlated, examining multiple metrics provides methodological robustness and could enable practitioners to select the most interpretable measure for their context—whether IR for clear min–max intuition, NECD for information-theoretic interpretation on a bounded scale, or CVCF for statistical dispersion. This convergent evidence enables practitioners to make evidence-based decisions about model suitability, training strategies, and expected performance ranges before committing to full-scale training and evaluation.

Traditional models showed gradual, approximately linear performance decline as imbalance increased, especially for high-cardinality targets, while deep models exhibited sharper, non-linear degradation patterns. Specifically, XGBoost variants consistently achieved the lowest ranks in our Friedman tests across both datasets (MIMIC-IV-ED:  $\chi^2(19, N = 45) = 737.91$ ,  $p = 3.30 \times 10^{-144}$ ; eICU:  $\chi^2(19, N = 40) = 506.85$ ,  $p = 2.04 \times 10^{-95}$ ), with performance degradation curves that maintained stability even at severe imbalance levels. These degradation patterns were consistent across all imbalance metrics, whether expressed as increasing IR and CVCF or decreasing NECD.

These performance decay patterns were reproducible across both datasets despite their differences. This cross-institutional consistency suggests that the relationship between model architecture and imbalance robustness reflects algorithmic properties rather than dataset-specific artifacts. The predictability of these patterns could enable proactive assessment of model suitability based on dataset characteristics, moving beyond trial-and-error approaches to evidence-based model selection.

An additional observation was that models trained without explicit weighting often achieved performance that was competitive with, and occasionally superior to, those using inverse or median frequency weighting. This can be attributed to two factors. First, ensemble methods such as XGBoost and Random Forest already mitigate imbalance through their recursive partitioning mechanisms, reducing the need for external reweighting. Second, aggressive weighting of very small classes may amplify noise, producing instability that offsets any gains in sensitivity. In contrast, the “effective number of samples” scheme consistently provided robust benefits across both datasets, likely because it moderates class contributions without overemphasizing extremely rare outcomes. These findings suggest that while effective weighting represents a reliable anchor point, forgoing weighting strategies remain a surprisingly strong baseline in high-data regimes where minority classes still have adequate representation.

### Empirical Scaling Relationships for Computational Efficiency

Training time analyses highlighted consistent differences in computational efficiency across model families. Tree-based methods, such as decision trees and random forests, remained computationally efficient, with training times increasing fairly steadily with dataset size (MIMIC-IV-ED:  $\chi^2(19, N = 15) = 321.66$ ,  $p = 7.12 \times 10^{-57}$ ; eICU:  $\chi^2(19, N = 15) = 244.54$ ,  $p = 3.93 \times 10^{-41}$ ). In contrast, neural architectures such as TabNet and TabResNet exhibited substantially higher training times, with evidence of higher growth that becomes prohibitive as dataset size grows. Weighting strategies did not materially alter computational cost, indicating that efficiency is largely determined by model architecture rather than class reweighting.



These scaling patterns have practical implications for deployment. In acute care environments, models often require retraining or continual learning as patient populations shift periodically, during public health emergencies, or when clinical practices evolve. Our results suggest that while deep tabular models may be computationally feasible in smaller pilot studies, their training requirements escalate rapidly at larger scales, in contrast to the relatively stable scaling of tree-based methods. This distinction provides healthcare systems with a basis for anticipating resource demands, moving beyond rough estimates or vendor specifications toward principled capacity planning.

### **An Examination of Assumptions About Architectural Complexity**

TabResNet architecture frequently outperformed TabNet while requiring significantly fewer computational resources across all prediction tasks and datasets. This finding questions the prevalent assumption (and hype) in DL research that more sophisticated architectures necessarily yield better performance, particularly in healthcare applications.

The sequential attention mechanism in TabNet, while theoretically elegant, appears to provide limited practical benefit for tabular healthcare data relative to its computational cost. TabResNet's residual connections without attention achieved comparable or superior representational capacity while maintaining computational efficiency compatible with real-time clinical workflows. This suggests that the architectural principles successful in computer vision and natural language processing may need further considerations before transfer directly to structured healthcare data.

From a clinical deployment viewpoint, TabResNet occupies a valuable middle ground: it offers the flexibility of DL architectures for potential multimodal integration while avoiding the computational penalties that make TabNet nearly economically prohibitive for large-scale deployment especially in low-resource settings.

### **Cross-Institutional Generalizability and Its Implications**

The consistency of performance patterns we have observed between MIMIC-IV-ED (single-center) and eICU (multicenter) databases point towards potential for clinical AI utility. Healthcare AI systems frequently fail when deployed outside their training environment due to population drift, documentation differences, or institutional practices. Our results suggest that the relative advantages of different model architectures—particularly ensemble robustness to class imbalance—generalize well and could pave the way towards multi-cohort validation, i.e., training on MIMIC-IV-ED and testing on eICU or vice versa. However, such a scenario would require considerable standardization and harmonization of the databases to enable such evaluations.

This could have implications for federated learning approaches and multi-institutional AI collaboratives. Rather than requiring extensive local validation for each model type, healthcare systems can leverage real-world evidence from other institutions to inform architecture selection. The reproducibility we showed could potentially reduce the barrier to adoption and supports the development of standardized approaches to clinical AI deployment.

However, this applies to relative performance patterns rather than absolute performance levels. While XGBoost consistently outperformed TabNet across institutions, the absolute F1 scores varied between datasets or even tasks on the same dataset, reflecting differences in patient complexity, outcome prevalence, and data quality. Local calibration and validation remain complementary and indispensable even when leveraging cross-institutional evidence for architecture selection.

### **Clinical and Translational Implications for Emergency and Critical Care**

Our findings suggest that traditional ensemble tree-based methods demonstrate comparatively robust performance under class imbalance, which may support more reliable detection of rare but clinically important outcomes. In the disposition prediction task, for example, improved recognition of patients at risk of in-hospital death or requiring urgent transfer could help reduce missed escalations. Similarly, in diagnosis prediction, where many categories are sparsely represented, robustness under imbalance may reduce the likelihood of overlooking uncommon yet serious conditions. In the eICU setting, the relatively stable performance of ensembles on mortality and severity tasks suggests potential utility in identifying patients who might benefit from intensified monitoring or prioritized allocation of resources. These potential implications remain speculative, as our analyses are retrospective and would need prospective validation in live clinical environments.

Beyond acute deterioration, predictive accuracy may also carry operational implications. Fewer false discharges could, in principle, lower the risk of avoidable readmissions, while more consistent identification of low-risk patients may help optimize admissions and resource allocation. The cross-institutional consistency observed in our experiments indicates that such patterns might be reproducible across different hospitals, but further work is required to establish generalizability in diverse clinical settings.

To place these results in context, it is useful to compare them with established clinical scoring systems. For mortality prediction, our optimized models achieved F1 scores of 0.75–0.90, which are numerically comparable to published discrimination for Acute Physiology and Chronic Health Evaluation II (APACHE II, AUC 0.80–0.85)<sup>42,43</sup> and Sequential Organ Failure Assessment (SOFA, AUC 0.69–0.92), as well as delta SOFA (AUC 0.51–0.83)<sup>44–46</sup>. Unlike manual, episodic scoring systems, ML models can in principle leverage continuously updated EHR data for dynamic risk assessment. For disposition prediction, performance (F1 0.70–0.80) was broadly aligned with reported accuracies for clinician gestalt (60–75%). These parallels should

not be interpreted as direct head-to-head comparisons, since the underlying cohorts, covariates, and evaluation metrics differ substantially between our study and those used in the development of APACHE II and SOFA. Rather, they provide approximate contextual benchmarks to situate the magnitude of our results within established clinical practice.

Looking beyond benchmarks, the potential benefits of robustness and computational efficiency may not be restricted to single institutions. The consistent relative performance patterns observed across MIMIC-IV-ED and eICU suggest that certain model families might generalize across healthcare systems, though this requires confirmation in non-U.S. and prospective contexts. The scalability of ensemble methods, in particular, may make them attractive for scenarios requiring frequent retraining or continual learning (e.g., seasonal variation or practice changes) or deployment in resource-constrained environments.

At the same time, predictive accuracy and computational scalability alone are insufficient to guarantee clinical utility. Successful translation into practice requires integration into complex workflows. Figure 9 illustrates one possible system architecture in which real-time data streams feed into predictive models, but this remains conceptual rather than validated. Safe and effective deployment will depend on integration with existing Information Technology (IT) systems, alignment with clinician workflows, and governance structures that ensure continuous monitoring, (re)calibration, and safety oversight.

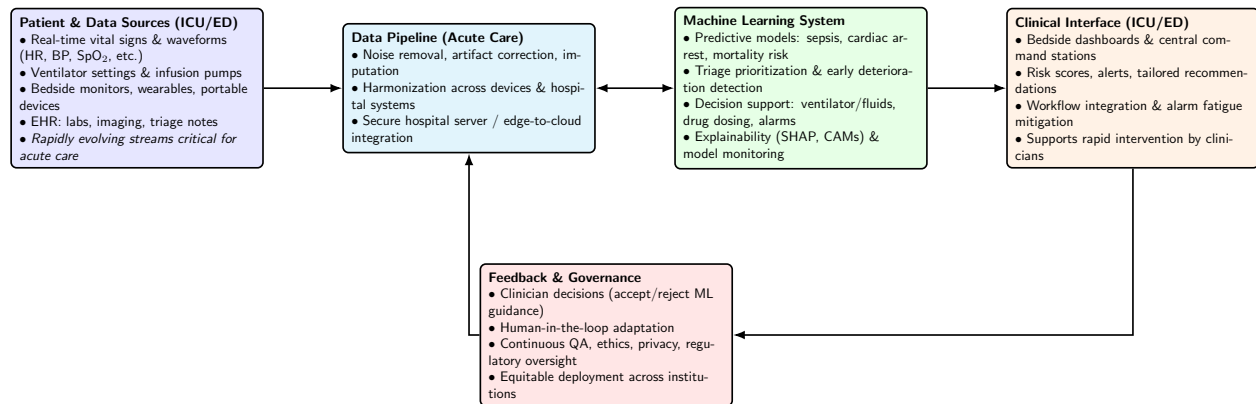


**Figure 9. Conceptual system architecture for AI-enabled clinical decision support.** An overview of a ML-enabled clinical decision support system for ICU and ED care. Archival and/ or real-time data streams from monitors, ventilators, infusion pumps, and EHRs feed into predictive models for tasks such as mortality prediction, disposition, and triage prioritization. Model outputs are delivered through clinician-facing dashboards with feedback and governance mechanisms to support safe, equitable, and workflow-aligned deployment.

Interpretability and clinician trust are also central considerations. Amongst ML model families, tree-based ensembles produce decision rules that can be more readily explained to stakeholders such as clinicians and regulators. Nonetheless, robustness alone is insufficient: poorly integrated systems risk contributing to alert fatigue or workflow disruption. Human-centered design, clinician feedback, and organizational change management must accompany algorithm development.

Finally, equity considerations are inseparable from technical ones. Class imbalance often reflects disparities in disease prevalence or access to care, and models that degrade under imbalance risk amplifying such inequities. By maintaining more stable performance across imbalance levels, ensemble approaches may help mitigate this risk. Their reproducibility across datasets further supports the potential for federated or collaborative approaches, although the equity implications of cross-institutional deployment remain to be systematically assessed.

Taken together, these observations highlight that model choice in clinical AI cannot be based on accuracy alone. Robustness to imbalance, computational scalability, interpretability, and governance considerations should all be treated as prerequisites for safe, equitable, and clinically meaningful deployment in emergency and critical care.

Building on these conceptual requirements, it is equally important to examine the practical realities of translating such models into routine use. Beyond demonstrating predictive accuracy in retrospective datasets, real-world deployment raises operational, technical, and regulatory challenges that must be addressed to ensure safety and sustainability.

## Operational Deployment and Implementation Considerations

Successful clinical deployment of these models requires addressing several operational and regulatory considerations beyond predictive performance. Model maintenance in clinical environments demands automated monitoring for *concept drift* as patient populations, clinical practices, and documentation patterns evolve. The computational efficiency of ensemble methods facilitates more frequent model retraining or *iterative finetuning* (e.g., freezing earlier layers and updating only the penultimate

or output layers, or adding new trainable layers on top of a fixed backbone) compared to ML approaches that may require substantial computational resources for updates.

Beyond maintenance, integration with existing hospital IT infrastructure presents both technical and workflow challenges. Models must interface with heterogeneous EHR platforms, respect institutional governance policies, and provide outputs in formats compatible with clinical decision support systems. The interpretability advantages of tree-based methods also align with regulatory requirements for algorithmic transparency in healthcare, potentially streamlining approval processes compared to “black-box” DL alternatives.

Even when technically integrated, models can fail if they disrupt workflows. Alert fatigue remains a critical deployment barrier: excessive or poorly calibrated warnings risk undermining clinician trust and efficiency<sup>47,48</sup>. Our models’ performance on minority classes could reduce false alerts, but implementation will require careful threshold tuning to balance sensitivity for critical events against specificity to minimize inappropriate notifications. The demonstrated cross-institutional consistency suggests that threshold settings established at one institution may transfer to others with minimal recalibration, though this requires prospective confirmation.

Beyond technical adjustments, organizational readiness and change management are essential. Clinicians need training on how to interpret AI outputs, with emphasis that predictions are designed to augment rather than replace clinical judgment. Governance frameworks should establish clear protocols for oversight, performance monitoring, and human override capabilities. Here again, the computational efficiency of ensembles supports rapid updates in response to performance degradation or evolving clinical needs, enabling a responsive rather than static approach to AI deployment.

Finally, privacy and security considerations cut across all stages of implementation. Models operating on streaming clinical data require robust safeguards for data handling and storage. The current efficiency of ensemble methods enables edge deployment options that minimize data transmission while maintaining real-time predictive capacity, potentially addressing institutional concerns about reliance on cloud-based AI services in healthcare settings.

## Equity, Fairness, and Bias Considerations

Class imbalance in healthcare data often reflects underlying disparities in access, disease prevalence, or clinical recognition patterns that can amplify existing inequities if not carefully addressed. Our evaluation provides evidence that ensemble methods maintain more consistent performance across different imbalance levels, which may translate to more equitable outcomes across patient subgroups.

However, overall robustness to class imbalance does not guarantee equitable performance across demographic groups. The minority classes in our prediction tasks (rare diagnoses, adverse outcomes) may themselves be distributed unequally across patient populations defined by race, sex, socioeconomic status, or geographic location. A model that performs well on aggregate imbalanced data might still exhibit significant disparities when evaluated within demographic subgroups.

Thus, a potential future avenue could be explicitly *evaluating subgroup-specific performance* and incorporating *fairness-aware metrics* into model development and validation processes. The computational efficiency advantages of ensemble methods we demonstrate could facilitate more comprehensive fairness evaluation by enabling rapid retraining and testing across different demographic stratifications.

*Roadmap for fairness evaluation and mitigation.* Building on this motivation, a *roadmap for fairness evaluation and possible bias mitigation* could include several steps. Subgroup analyses may not always be feasible in initial model development, but efficiency advantages of ensemble methods make them well-suited for rapid retraining across multiple stratifications once additional data become available. In practice, fairness assessment could involve (i) reporting group-wise discrimination (e.g., AUROC, AUPRC) and error rates (FNR/FPR), (ii) evaluating calibration and threshold-dependent equity criteria (e.g., equal opportunity), (iii) analyzing intersectional strata (e.g., sex  $\times$  age, race/ethnicity  $\times$  insurance status) to surface compound disparities, and (iv) iteratively applying mitigation strategies such as group-aware thresholding, or post-hoc calibration with continuous drift monitoring in deployment.

At the same time, technical fairness evaluations must be interpreted within the broader context of health equity, as algorithmic fairness metrics alone cannot capture the structural and institutional drivers of disparity<sup>49–52</sup>. The deployment advantages of ensemble methods—computational efficiency, cross-institutional generalizability—highlight their potential for broad adoption. However, systemic risks remain: if deployment decisions are shaped primarily by institutional resources rather than clinical appropriateness, inequities could emerge. For example, if resource-constrained hospitals systematically receive “lighter” models while better-funded centers deploy more experimental or bespoke systems, differences in access to innovation and long-term support could inadvertently reinforce disparities, even if the immediate predictive performance of ensemble models is strong.

## Contextualization With Existing Literature

This study builds on and aligns with prior research underscoring the effectiveness of tree-based methods on tabular data<sup>16,37</sup>. Our contribution extends this work by systematically evaluating models under controlled imbalance conditions and quantifying

scaling relationships specifically in ED/ICU care clinical contexts.

Whereas earlier comparisons of DL and traditional methods on healthcare data have often been restricted to specific clinical domains or single datasets<sup>21,53</sup>, our cross-institutional validation across both emergency department and intensive care settings provides broader evidence for the generalizability of ensemble advantages under imbalance.

In addition to these comparative results, we introduce an architectural contribution. The TabResNet model builds on established principles of residual learning<sup>54</sup> but adapts them specifically for tabular healthcare data under computational efficiency constraints. While not a theoretical breakthrough, this design represents a practical addition to the toolkit of clinical AI practitioners who require DL capabilities without the resource demands of trendy transformer-based counterparts.

We also advance methodological clarity through our systematic approach to imbalance quantification. By combining multiple complementary metrics (CVCF, IR, NECD), we provide a more comprehensive framework. This allows a more nuanced understanding of how different aspects of class distribution affect model performance.

## **Limitations and Future Research Directions**

A few limitations constrain the generalizability of our study and suggest potential directions for future work.

### ***Scope of Data Modalities***

This study focused exclusively on structured EHR data, where ensemble methods have established advantages. Healthcare AI is increasingly evolving towards multimodal data integration, combining structured records with medical imaging, genomic, clinical notes, and physiological time series. Deep architectures may recover their advantages when applied to these richer data modalities, and the scaling relationships we observed may not hold for multimodal systems.

### ***Imbalance Mitigation Strategies***

Our approach to addressing class imbalance decidedly utilized class weighting strategies that can be applied consistently across model architectures. This methodological choice enabled fair comparison but may have inadvertently disadvantaged DL methods that could benefit from specialized techniques like focal loss<sup>26</sup>, progressive resampling, or adversarial training approaches designed for neural networks.

### ***Temporal Dynamics and Streaming Data***

Our evaluation used static datasets that do not capture the temporal dynamics of real clinical environments. Patient populations evolve continuously, seasonal patterns affect disease prevalence, and clinical practices change over time. The scaling relationships and performance patterns we observed may differ when models must adapt to streaming data with evolving class distributions.

### ***Clinical Integration and Human Factors***

While we discussed deployment considerations, our evaluation was conducted entirely in retrospective settings. The performance advantages of ensemble methods may be offset by other factors such as clinician acceptance, workflow integration challenges, or regulatory requirements that favor different architectural approaches.

### ***Fairness and Subgroup Analysis***

Our current analysis focused on overall performance across clinical tasks and did not examine potential disparities across demographic subgroups. A clear direction for future research is to evaluate whether the robustness advantages of ensemble methods also translate into equitable performance across patient populations defined by race, sex, age, socioeconomic status, and other relevant characteristics. Such investigations could involve stratified fairness audits with group-wise metrics, intersectional analyses, calibration checks, and mitigation strategies (e.g., cost-sensitive reweighting, group-aware thresholding), leveraging the retraining efficiency of ensemble models to iterate rapidly across subgroups. We therefore acknowledge the absence of subgroup-specific analyses as a limitation of the present study and highlight fairness evaluation as an important next step.

### ***Geographic and Healthcare System Generalizability***

Questions of fairness intersect closely with questions of context. While subgroup analyses address which patient populations models serve equitably, geographic and institutional diversity determines where such models can be trusted. Both MIMIC-IV-ED and eICU represent academic medical centers in the United States with specific patient populations, clinical practices, and documentation standards. The generalizability of our findings to community hospitals, international healthcare systems, or resource-constrained settings remains to be established.

Future research should address these limitations holistically: through prospective validation studies that evaluate model performance in live clinical workflows, comprehensive fairness analyses across demographic subgroups, and extension to multimodal healthcare AI systems. Additionally, investigation of hybrid architectures that combine the robustness of ensemble methods with the representational capacity of deep learning for specific modalities represents a promising direction for clinical AI development.

## Conclusion

This study systematically evaluated the robustness and scalability of classical and deep learning approaches for imbalanced tabular data in emergency and critical care. Across two large-scale EHR datasets, ensemble methods, especially XGBoost, consistently maintained superior predictive performance and computational efficiency under increasing imbalance, while deep tabular models showed sharper degradation and higher training costs. The proposed TabResNet architecture offered a computationally lighter alternative to attention-based models, but did not surpass ensemble benchmarks.

By quantifying imbalance with three complementary metrics, we demonstrated that predictive degradation patterns are reproducible across datasets and consistent across metrics, with CVCF adding nuance in high-cardinality tasks. Importantly, the purpose of this work is not methodological novelty, but to provide practitioners with an evidence-based framework for selecting models that balance predictive robustness, scalability, and clinical feasibility.

Our findings suggest that ensemble methods currently represent the most practical choice for ED and ICU deployment, where reliability and computational efficiency are paramount. Future work should extend this framework to multimodal data integration, prospective validation, and cross-institutional collaborations to ensure that AI systems for acute care remain robust, equitable, and aligned with clinical workflows.

## References

1. Huang, Q., Thind, A., Dreyer, J. F. & Zaric, G. S. The impact of delays to admission from the emergency department on inpatient outcomes. *BMC emergency medicine* **10**, 16 (2010).
2. Carayon, P., Xie, A. & Kianfar, S. Human factors and ergonomics as a patient safety practice. *BMJ Qual. & Saf.* **23**, 196–205 (2014).
3. Weigl, M., Müller, A., Vincent, C., Angerer, P. & Sevdalis, N. The association of workflow interruptions and hospital doctors' workload: a prospective observational study. *BMJ quality & safety* **21**, 399–407 (2012).
4. Johnson, A. E. *et al.* Machine learning and decision support in critical care. *Proc. IEEE* **104**, 444–466 (2016).
5. Komorowski, M., Celi, L. A., Badawi, O., Gordon, A. C. & Faisal, A. A. The artificial intelligence clinician learns optimal treatment strategies for sepsis in intensive care. *Nat. medicine* **24**, 1716–1720 (2018).
6. Esteva, A. *et al.* A guide to deep learning in healthcare. *Nat. medicine* **25**, 24–29 (2019).
7. Topol, E. J. High-performance medicine: the convergence of human and artificial intelligence. *Nat. medicine* **25**, 44–56 (2019).
8. Rajpurkar, P., Chen, E., Banerjee, O. & Topol, E. J. Ai in health and medicine. *Nat. medicine* **28**, 31–38 (2022).
9. Miotto, R., Wang, F., Wang, S., Jiang, X. & Dudley, J. T. Deep learning for healthcare: review, opportunities and challenges. *Briefings bioinformatics* **19**, 1236–1246 (2018).
10. Jiang, F. *et al.* Artificial intelligence in healthcare: past, present and future. *Stroke vascular neurology* **2** (2017).
11. He, H. & Garcia, E. A. Learning from imbalanced data. *IEEE Transactions on Knowl. Data Eng.* **21**, 1263–1284, DOI: [10.1109/TKDE.2008.239](https://doi.org/10.1109/TKDE.2008.239) (2009).
12. Branco, P., Torgo, L. & Ribeiro, R. P. A survey of predictive modeling on imbalanced domains. *ACM Comput. Surv.* **49**, 31:1–31:50, DOI: [10.1145/2907071](https://doi.org/10.1145/2907071) (2016).
13. LeCun, Y., Bengio, Y. & Hinton, G. Deep learning. *Nature* **521**, 436–444 (2015).
14. Krizhevsky, A., Sutskever, I. & Hinton, G. E. Imagenet classification with deep convolutional neural networks. In *Advances in Neural Information Processing Systems*, vol. 25 (2012).
15. Silver, D. *et al.* Mastering the game of go without human knowledge. *Nature* **550**, 354–359 (2017).
16. Shwartz-Ziv, R. & Armon, A. Tabular data: Deep learning is not all you need. *Inf. Fusion* **81**, 84–90 (2022).
17. Liu, X., Wu, J. & Zhou, Z.-H. Deep learning in medical image analysis: Challenges and applications. *Med. Image Analysis* **67**, 101819, DOI: [10.1016/j.media.2020.101819](https://doi.org/10.1016/j.media.2020.101819) (2020).
18. Rajkomar, A. *et al.* Scalable and accurate deep learning with electronic health records. *NPJ Digit. Medicine* **1**, DOI: [10.1038/s41746-018-0029-1](https://doi.org/10.1038/s41746-018-0029-1) (2018).
19. Chen, T. & Guestrin, C. Xgboost: A scalable tree boosting system. In *Proceedings of the 22nd ACM SIGKDD International Conference on Knowledge Discovery and Data Mining*, 785–794, DOI: [10.1145/2939672.2939785](https://doi.org/10.1145/2939672.2939785) (2016).
20. Lundberg, S. M. *et al.* Explainable ai for trees: From local explanations to global understanding. *Nat. Mach. Intell.* **2**, 56–67, DOI: [10.1038/s42256-019-0138-9](https://doi.org/10.1038/s42256-019-0138-9) (2020).



21. Choi, E., Schuetz, A., Stewart, W. F. & Sun, J. Using recurrent neural network models for early detection of heart failure onset. *J. Am. Med. Informatics Assoc.* **24**, 361–370, DOI: [10.1093/jamia/ocw112](https://doi.org/10.1093/jamia/ocw112) (2017).
22. Katuwal, G. J. & Chen, J. Feature selection and classification methods for imbalanced cancer datasets. *PLoS ONE* **11**, e0157853, DOI: [10.1371/journal.pone.0157853](https://doi.org/10.1371/journal.pone.0157853) (2016).
23. Luo, Y., Szolovits, P., Dighe, A. & Baron, J. M. Using machine learning to predict laboratory test results. *Am. J. Clin. Pathol.* **145**, 778–788, DOI: [10.1093/ajcp/aqw155](https://doi.org/10.1093/ajcp/aqw155) (2016).
24. Chawla, N. V., Bowyer, K. W., Hall, L. O. & Kegelmeyer, W. P. Smote: synthetic minority over-sampling technique. *J. artificial intelligence research* **16**, 321–357 (2002).
25. Elkan, C. The foundations of cost-sensitive learning. In *International joint conference on artificial intelligence*, vol. 17, 973–978 (Lawrence Erlbaum Associates Ltd, 2001).
26. Lin, T.-Y., Goyal, P., Girshick, R., He, K. & Dollár, P. Focal loss for dense object detection. In *Proceedings of the IEEE international conference on computer vision*, 2980–2988 (2017).
27. Buda, M., Maki, A. & Mazurowski, M. A. A systematic study of the class imbalance problem in convolutional neural networks. *Neural Networks* **106**, 249–259, DOI: [10.1016/j.neunet.2018.07.011](https://doi.org/10.1016/j.neunet.2018.07.011) (2018).
28. Arik, S. O. & Pfister, T. Tabnet: Attentive interpretable tabular learning. *Proc. AAAI Conf. on Artif. Intell.* **35**, 6679–6687, DOI: [10.1609/aaai.v35i8.16665](https://doi.org/10.1609/aaai.v35i8.16665) (2021).
29. Johnson, A. *et al.* Mimic-iv-ed. *PhysioNet* (2021).
30. Goldberger, A. L. *et al.* Physiobank, physiotoolkit, and physionet: components of a new research resource for complex physiologic signals. *circulation* **101**, e215–e220 (2000).
31. Pollard, T. *et al.* eicu collaborative research database (version 2.0). *PhysioNet* DOI: [10.13026/C2WM1R](https://doi.org/10.13026/C2WM1R) (2019).
32. Quinlan, J. R. Induction of decision trees. In *Machine Learning*, vol. 1, 81–106 (Springer, 1986).
33. Breiman, L. *Random Forests*, vol. 45 (Machine Learning, 2001).
34. Chen, T. & Guestrin, C. Xgboost: A scalable tree boosting system. In *Proceedings of the 22nd ACM SIGKDD International Conference on Knowledge Discovery and Data Mining*, 785–794 (ACM, 2016).
35. Ke, G. *et al.* Lightgbm: A highly efficient gradient boosting decision tree. *Adv. neural information processing systems* **30** (2017).
36. Prokhorenkova, L., Gusev, G., Vorobev, A., Dorogush, A. V. & Gulin, A. Catboost: unbiased boosting with categorical features. *Adv. neural information processing systems* **31** (2018).
37. Grinsztajn, L., Oyallon, E. & Varoquaux, G. Why do tree-based models still outperform deep learning on typical tabular data? *Adv. neural information processing systems* **35**, 507–520 (2022).
38. Arik, S. Ö. & Pfister, T. Tabnet: Attentive interpretable tabular learning. In *Proceedings of the AAAI conference on artificial intelligence*, vol. 35, 6679–6687 (2021).
39. Hollmann, N., Müller, S., Eggensperger, K. & Hutter, F. TabPFN: A transformer that solves small tabular classification problems in a second. *arXiv preprint arXiv:2207.01848* (2022).
40. Cui, Y., Jia, M., Lin, T.-Y., Song, Y. & Belongie, S. Class-balanced loss based on effective number of samples. In *Proceedings of the IEEE/CVF conference on computer vision and pattern recognition*, 9268–9277 (2019).
41. Akiba, T., Sano, S., Yanase, T., Ohta, T. & Koyama, M. Optuna: A next-generation hyperparameter optimization framework. In *Proceedings of the 25th ACM SIGKDD international conference on knowledge discovery & data mining*, 2623–2631 (2019).
42. Lee, H., Shon, Y.-J., Kim, H., Paik, H. & Park, H.-P. Validation of the apache iv model and its comparison with the apache ii, saps 3, and korean saps 3 models for the prediction of hospital mortality in a korean surgical intensive care unit. *Korean journal anesthesiology* **67**, 115 (2014).
43. Badrinath, K. *et al.* Comparison of various severity assessment scoring systems in patients with sepsis in a tertiary care teaching hospital. *Indian journal critical care medicine: peer-reviewed, official publication Indian Soc. Critical Care Medicine* **22**, 842 (2018).
44. Minne, L., Abu-Hanna, A. & de Jonge, E. Evaluation of sofa-based models for predicting mortality in the icu: A systematic review. *Critical care* **12**, R161 (2008).

45. Bosch, N. A., Law, A. C., Rucci, J. M., Peterson, D. & Walkey, A. J. Predictive validity of the sequential organ failure assessment score versus claims-based scores among critically ill patients. *Annals Am. Thorac. Soc.* **19**, 1072–1076 (2022).
46. Asmarawati, T. P. *et al.* Predictive value of sequential organ failure assessment, quick sequential organ failure assessment, acute physiology and chronic health evaluation ii, and new early warning signs scores estimate mortality of covid-19 patients requiring intensive care unit. *Indian J. Critical Care Medicine: Peer-reviewed, Off. Publ. Indian Soc. Critical Care Medicine* **26**, 464 (2022).
47. Ancker, J. S. *et al.* Effects of workload, work complexity, and repeated alerts on alert fatigue in a clinical decision support system. *BMC medical informatics decision making* **17**, 36 (2017).
48. Chaparro, J. D. *et al.* Clinical decision support stewardship: best practices and techniques to monitor and improve interruptive alerts. *Appl. Clin. Informatics* **13**, 560–568 (2022).
49. Donini, M., Oneto, L., Ben-David, S., Shawe-Taylor, J. S. & Pontil, M. Empirical risk minimization under fairness constraints. *Adv. neural information processing systems* **31** (2018).
50. Oneto, L., Donini, M. & Pontil, M. General fair empirical risk minimization. In *2020 International Joint Conference on Neural Networks (IJCNN)*, 1–8 (IEEE, 2020).
51. Abràmoff, M. D. *et al.* Considerations for addressing bias in artificial intelligence for health equity. *NPJ digital medicine* **6**, 170 (2023).
52. Sikstrom, L. *et al.* Conceptualising fairness: three pillars for medical algorithms and health equity. *BMJ health & care informatics* **29**, e100459 (2022).
53. Rajkomar, A. *et al.* Scalable and accurate deep learning with electronic health records. *NPJ digital medicine* **1**, 18 (2018).
54. He, K., Zhang, X., Ren, S. & Sun, J. Deep residual learning for image recognition. In *Proceedings of the IEEE conference on computer vision and pattern recognition*, 770–778 (2016).
55. Johnson, A., Pollard, T., Mark, R., Berkowitz, S. & Horng, S. MIMIC-CXR database. *PhysioNet10* **13026**, C2JT1Q (2024).

## Funding Statement

This research was supported in part by the National Research Foundation of South Africa (Ref No. CSRP23040990793).

## Author contributions statement

Y.B. conceived and designed the study, curated and preprocessed the datasets, implemented the machine learning models, performed the experiments, analyzed the results, and drafted the manuscript. M.A. contributed to the methodological design, supervised the work, assisted with interpretation of the findings, and provided critical revisions to the manuscript. All authors read and approved the final manuscript.

## Competing Interests

All authors declare no financial or non-financial competing interests.

## Data Availability

The datasets analyzed during the current study are freely available and hosted on PhysioNet. The MIMIC-IV-ED (v2.2), MIMIC-CXR (v2.1.0), and eICU Collaborative Research Database (v2.0) are available at <https://physionet.org/content/mimic-iv-ed/2.2/>, <https://physionet.org/content/mimic-cxr/2.1.0/>, and <https://physionet.org/content/eicu-crd/2.0/>, respectively. Access to these databases requires credentialing and completion of a data use agreement through PhysioNet. No new datasets were generated in this study.

## Code Availability

The code developed for this study is publicly available on GitHub at <https://github.com/yusufbrima/tabresnet>.

## **.1 Data Preprocessing and Feature Engineering**

### ***.1.1 MIMIC-IV-ED***

For the MIMIC-IV-ED cohort, we extracted structured electronic health records encompassing patient stays, triage assessments, diagnoses, and vital sign measurements. The initial cohort definition leveraged the MIMIC-CXR<sup>55</sup> core table to identify eligible patients and establish potential linkages with radiographic data. In this study, however, we focused our analysis to structured tabular information from the emergency department (ED), while noting that the multimodal potential of this resource remains valuable for future investigations.

Within this structured dataset, diagnostic information was standardized by reducing ICD codes to the three-character level, thereby capturing broader diagnostic categories in a clinically interpretable manner. For each ED stay, the first recorded diagnosis was designated as the primary label, and patient disposition at discharge was harmonized into four outcome categories (admitted, transferred, discharged, deceased) through a standardized mapping procedure.

In addition to diagnostic and outcome information, vital sign measurements were aggregated at the stay level to summarize temperature, heart rate, respiratory rate, oxygen saturation, and systolic/diastolic blood pressure. This approach reduced redundancy from repeated recordings while retaining clinically relevant signals. Demographic and ED-related variables (e.g., age, sex, race, mode of arrival, and acuity) were also preserved as predictors, providing contextual information about patient presentation.

To maintain data integrity, records were restricted to those with valid ICD codes and complete linkages between ED stays and diagnoses, and duplicate identifiers were removed to avoid overrepresentation. The resulting curated dataset consisted of identifiers, target variables (diagnoses, grouped ICD codes, discharge disposition), demographic attributes, ED-related features, and aggregated vital signs. After preprocessing, this streamlined and clinically interpretable EHR cohort provided a robust foundation for predictive modeling, while its multimodal structure points to future opportunities for integrating imaging with EHR data.

### ***.1.2 eICU Collaborative Research Database***

For this dataset, we constructed the cohort with careful attention to temporal leakage prevention. Core patient information, admission characteristics, diagnostic data, laboratory measurements, and periodic vital sign recordings were extracted. To ensure that models relied only on information available at clinically relevant decision points, we restricted measurements to the first 24 hours of ICU admission. Vital signs and laboratory results were filtered using time offsets, preventing any leakage from future observations.

Building on this temporal window, vital sign features were aggregated at the patient-stay level, with summary statistics (mean, standard deviation, minimum, maximum, and count) computed for variables such as temperature, oxygen saturation, heart rate, respiration rate, and blood pressure. Laboratory measurements were similarly constrained to the 20 most frequently ordered tests and summarized with equivalent statistics. Admission diagnoses were limited to those recorded at or before admission, and these were represented both as concatenated diagnosis strings and as diagnosis counts.

From these features, we derived a set of clinically meaningful target variables. Mortality risk was defined by combining ICU and hospital discharge status with length-of-stay thresholds, yielding outcome classes such as ICU death, hospital death, critical survivor, and routine discharge. Length of stay was categorized into five ordinal classes, ranging from very short (<24 h) to prolonged (>4 weeks). Clinical severity was operationalized via a composite score integrating indicators of organ support (e.g., ventilation, dialysis), circulatory compromise, neurological status (Glasgow Coma Scale), and metabolic derangement. Discharge disposition was harmonized into interpretable categories, including home/hospice, extended care facilities, ICU transfers, and death. Resource utilization was characterized by combining length of stay with high-intensity interventions, stratifying patients into four utilization tiers.

The final merged dataset brought together demographic variables, severity scores, interventions, aggregated vital signs, laboratory summaries, and diagnostic features alongside the constructed target variables. Data quality checks were applied to remove potential leakage columns (e.g., hospital discharge status), and records with missing target labels were excluded. Categorical variables, including gender, ethnicity, and diagnosis strings, were retained in their raw form to allow flexible encoding strategies. To facilitate downstream modeling, the processed datasets were saved in modular format, separating features, targets, and the complete merged dataset for streamlined machine learning pipelines.

### ***.1.3 Feature Normalization and Handling Missing Values***

To ensure comparability across heterogeneous clinical variables, continuous features were standardized to zero mean and unit variance prior to model training. Categorical features, including demographic indicators and diagnostic codes, were transformed via one-hot encoding to preserve discrete class membership without imposing ordinal assumptions. Missing values were addressed through simple but robust imputation strategies: continuous variables were imputed with the median, whereas categorical variables were imputed with the mode. To maintain data integrity, features with more than 50% missing data were

excluded from the analytic dataset. This procedure balances the trade-off between retaining as much information as possible and avoiding the introduction of excessive noise from sparsely observed features.

#### **.1.4 Train–Validation–Test Splits**

For both the MIMIC-IV-ED and eICU cohorts, we partitioned each into training, validation, and test sets with proportions of 60%, 20%, and 20%, respectively. Stratified sampling was applied to preserve the distribution of outcome classes across all subsets, thereby ensuring that rare but clinically important categories remained represented in both model development and evaluation. This strategy facilitated reliable performance assessment while guarding against biased estimates due to class imbalance.

#### **.1.5 Hyperparameter Optimization**

This section summarizes the hyperparameter search spaces, optimization procedures, and evaluation strategies applied across all the models. Optimization was performed with Optuna via the tree-structured Parzen estimator (TPE; seed=42) and the MedianPruner to terminate unpromising trials. Each model–dataset pair was tuned over 100 trials, and performance was consistently measured by the average F1 score on the validation set.

#### **.1.6 Traditional Machine Learning Models**

Decision trees were tuned over maximum depth (2–32), minimum samples per split (2–50), minimum samples per leaf (1–20), and splitting criterion (gini or entropy). Random forests varied in number of estimators (100–1000), depth (3–25), splitting parameters as above, and maximum features (sqrt, log2, or fixed fractions). XGBoost models were optimized for estimators (200–1200), learning rate (0.01–0.3), depth (3–12), subsampling (0.6–1.0), column sampling (0.5–1.0), and regularization terms ( $\alpha$  and  $\lambda$ , 0–5).

#### **.1.7 Deep Learning Models**

TabNet was tuned over learning rate ( $1 \times 10^{-6}$ – $1 \times 10^{-1}$ ), weight decay ( $1 \times 10^{-7}$ – $1 \times 10^{-2}$ ), and batch size (32–1024). The custom neural network (TabResNet) included these parameters plus the number of residual blocks (1–4), hidden dimensions (from half to twice the input size, bounded at 8–16), and an optional reduction layer.

#### **.1.8 Evaluation and Convergence**

For traditional models, hyperparameters were selected by training on the training split and evaluating on the validation split. Deep learning models followed the same scheme with early stopping: training halted after 15 epochs without validation improvement for TabResNet (configurable for TabNet), with the best checkpoint restored. A ReduceLROnPlateau scheduler reduced learning rates by a factor of 0.5 after three stagnant epochs.

#### **.1.9 Class Imbalance Handling**

To address class imbalance, weighting strategies were incorporated during optimization. For traditional models, class or sample weights were applied directly through implementation parameters. For deep learning, class weights were embedded in the loss function. We compared inverse frequency, median frequency, and effective number of samples (with  $\beta = 0.9999$ ), as well as unweighted baselines.

### **.2 MIMIC-IV-ED Results**

#### **.2.1 Training Time Scaling Plots**

Figure 10 provides extended analysis of training time scaling with dataset size for the MIMIC-IV-ED dataset. Each panel corresponds to one of the three prediction tasks: disposition outcomes, ICD code categories, and primary diagnosis. The training time is plotted on a logarithmic scale against the number of training samples, with curves shown for all classifiers and class weighting strategies. These plots complement the rank-based comparisons presented in the main text by highlighting absolute training time differences and scaling behavior across models. In particular, they illustrate the widening efficiency gap between tree-based ensembles and attention-based deep learning models as the dataset size increases.

### **.3 EICU Results**

Here, we present extended results for the eICU dataset, complementing the main text findings by providing detailed analyses of class imbalance metrics, classifier performance, and training time behavior across diverse prediction tasks. The figures included here are intended to provide additional depth, showing how different models and weighting strategies perform across mortality risk, length of stay, severity, discharge disposition, and resource utilization outcomes.

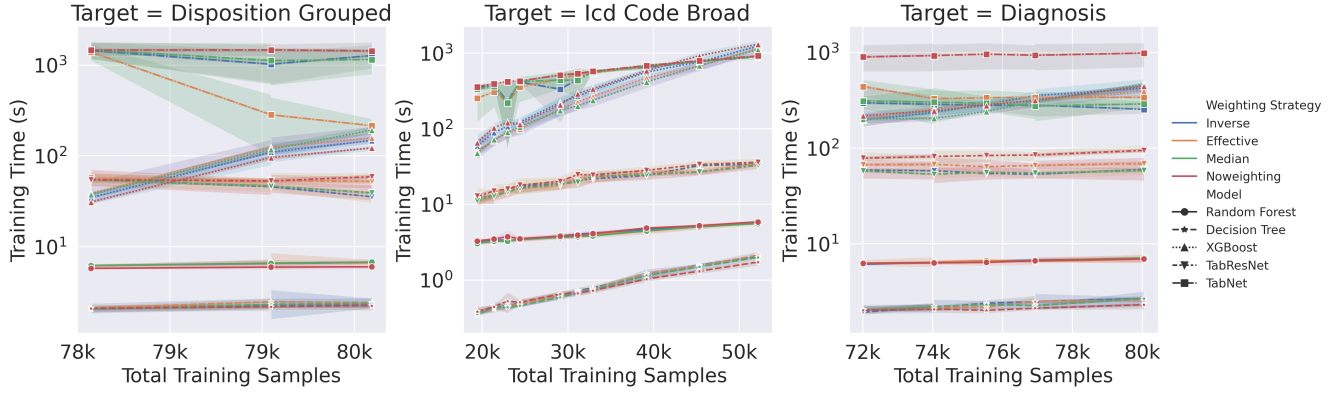


**Figure 10. Computational scaling across model architectures.** Training time as a function of dataset size for different prediction tasks. Each panel shows the training time (seconds, log scale) versus the total number of training samples for a specific target variable. The results are reported across all classifiers and class weighting strategies.

### .3.1 Correlation of Class Imbalance Metrics

Figure 11 shows the pairwise correlations between the CVCF, IR, and NECD for different weighting strategies. NECD was inversely correlated with IR and CVCF, providing a bounded and interpretable measure of overall class distributional uncertainty. The patterns were consistent across tasks, confirming that these measures capture related but complementary aspects of imbalance severity.

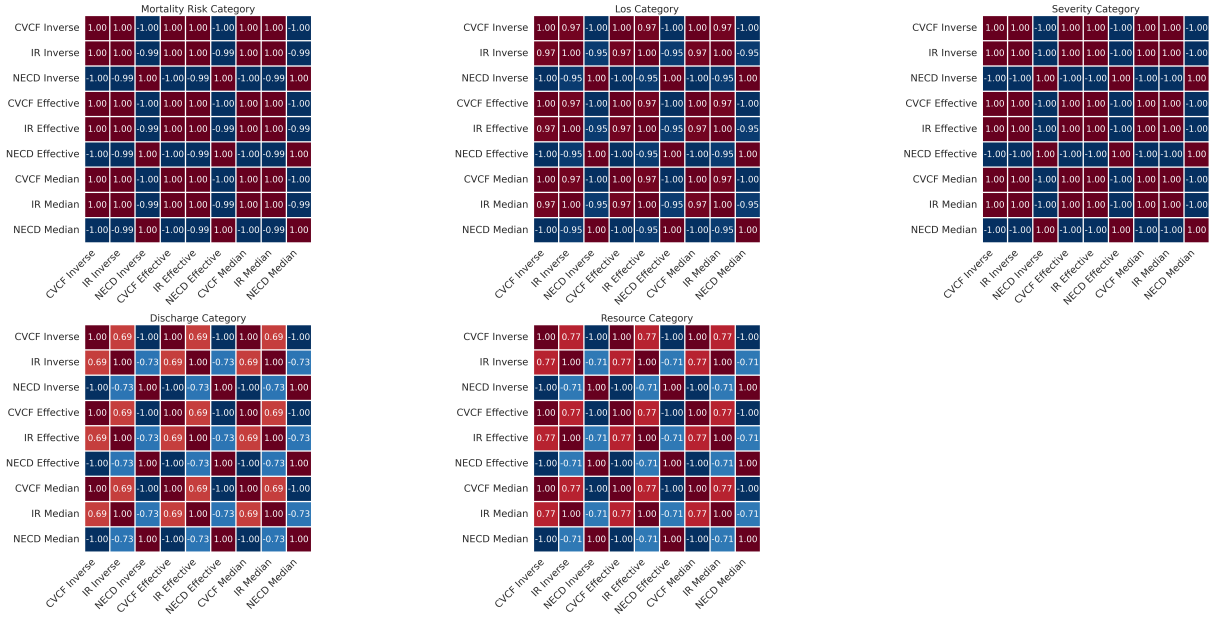


**Figure 11. Correlation heatmaps of class imbalance metrics for five prediction tasks.** As in MIMIC, all three measures were strongly aligned in low-cardinality outcomes (mortality, LOS, severity). In higher-cardinality tasks (discharge, resource utilization), correlations between CVCF and the other two measures were somewhat weaker, reflecting its greater sensitivity to distributional spread across many moderately rare classes. Nevertheless, CVCF remained directionally consistent with IR and NECD, indicating that all three metrics provide a coherent characterization of imbalance severity across diverse label spaces.

### .3.2 Classifier Performance Comparison

We compared the predictive performance (weighted F1 score) of 20 classifiers across multiple experimental blocks, with each block corresponding to a unique combination of a target variable and a training set size. A Friedman test indicated significant differences among classifiers ( $\chi^2(19, N = 45) = 506.85, p = 2.04 \times 10^{-95}$ ). Post-hoc pairwise comparisons with Wilcoxon signed-rank tests and Holm correction (Figure 12) showed that XGBoost variants consistently achieved the lowest average ranks,



reflecting superior predictive performance, followed by Random Forest and Decision Tree variants. By contrast, TabResNet and TabNet variants obtained higher ranks, indicating comparatively poorer performance on the eICU dataset. Across all tasks, performance degradation curves were consistent across imbalance measures: higher IR and CVCF values, or lower NECD values (approaching 0 from 1), were associated with declines in weighted F1.

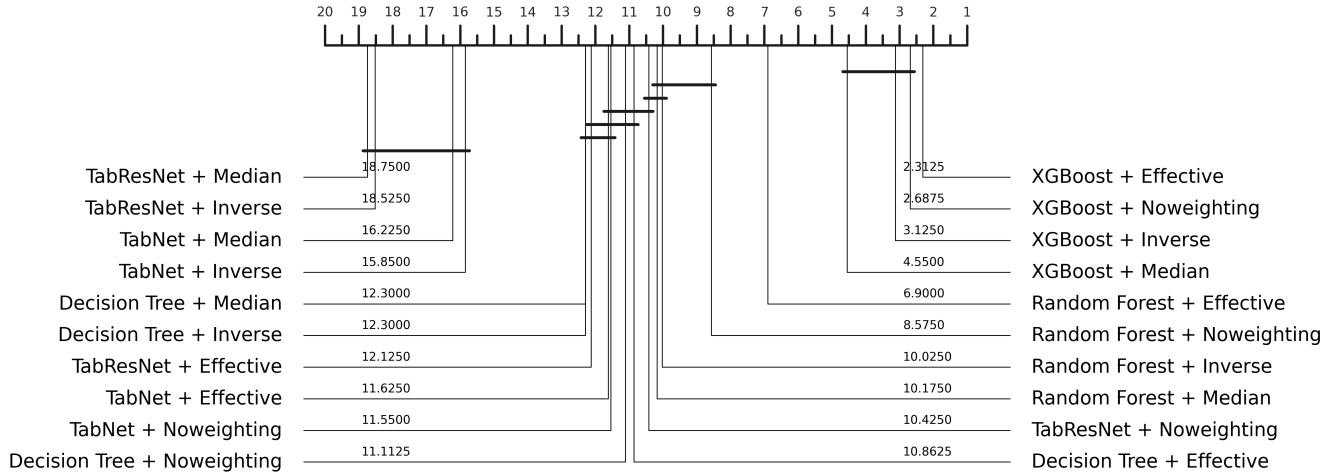


**Figure 12. Classifier performance rankings across experimental conditions.** Critical difference diagram showing the average ranks of 20 classifiers on the eICU dataset on the basis of their weighted F1 scores across experimental blocks. Lower ranks indicate better predictive performance. The classifiers connected by a horizontal bar are not significantly different according to Wilcoxon signed-rank tests with Holm correction.

Extended results for individual prediction tasks are shown in Figures 13–17, highlighting how model performance varies with imbalance severity across discharge disposition, length of stay, mortality risk, resource utilization, and clinical severity.

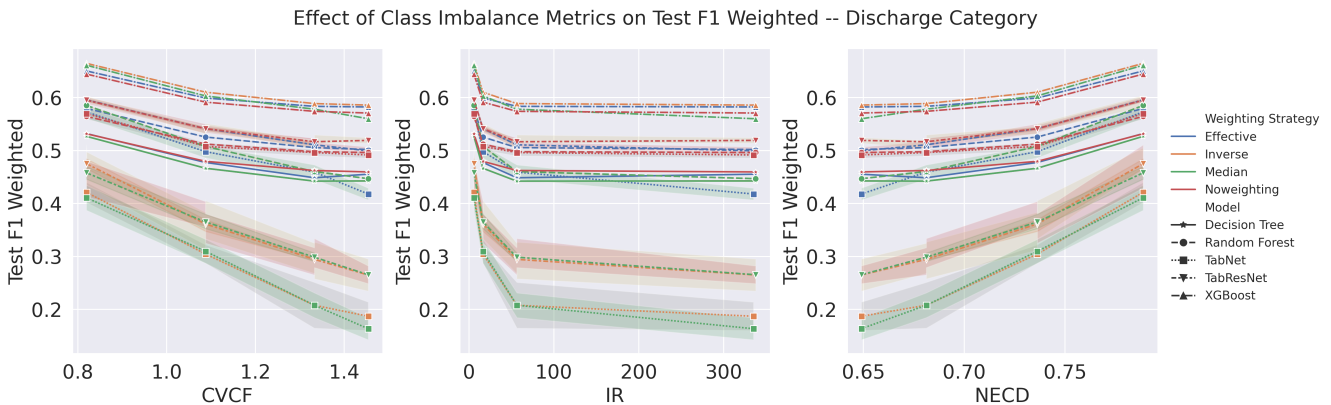


**Figure 13. Impact of class imbalance on discharge disposition prediction.** Weighted F1 outcomes for five model families (Decision Tree, Random Forest, TabNet, TabResNet, XGBoost) under four weighting strategies (none, inverse, effective number, median). Performance trends are shown with respect to three imbalance measures. Tree-based ensemble approaches, particularly XGBoost, displayed the most robust performance across imbalance levels, while deep models showed steeper declines. CVCF trends were directionally consistent with those from IR and NECD.

### .3.3 Training Time Comparison

We compared the training times of 20 classifiers across 40 experimental blocks, where each block corresponds to a unique combination of a target variable and a training set size. A Friedman test revealed a statistically significant difference in training times among the classifiers ( $\chi^2(19, N = 40) = 244.54, p = 3.93 \times 10^{-41}$ ). Post-hoc pairwise comparisons using Wilcoxon signed-rank tests with Holm correction (Figure 18) showed that the Decision Tree variants achieved the lowest average ranks

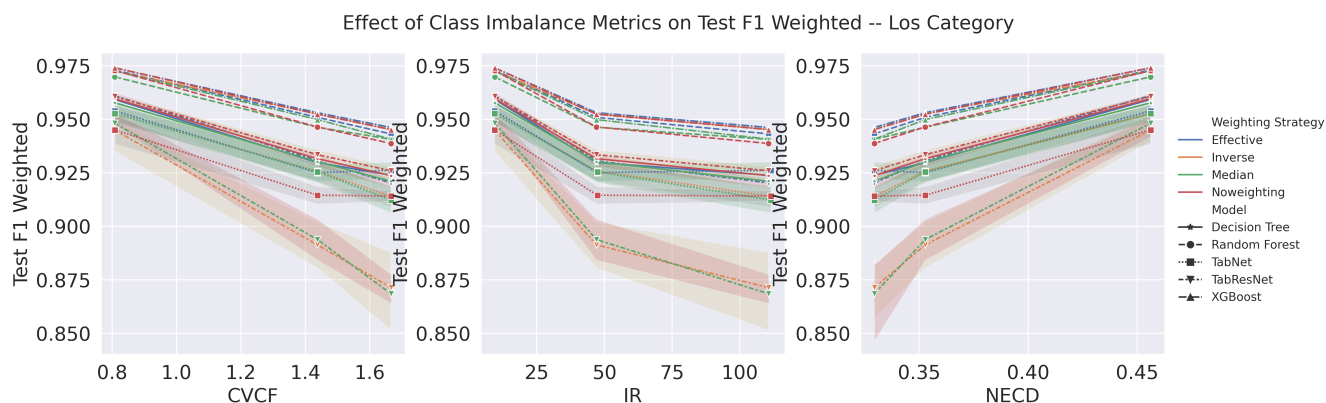


**Figure 14. Class imbalance and length-of-stay prediction.** Weighted F1 trajectories for the same model families across different weighting strategies, plotted against CVCF, IR, and NECD. Although performance gradually decreased with stronger imbalance, overall F1 scores remained relatively high. XGBoost and Random Forest retained stable accuracy, while TabNet and TabResNet were more affected at higher skew levels. The three imbalance metrics produced closely aligned degradation curves, with NECD decreasing monotonically as imbalance increased.

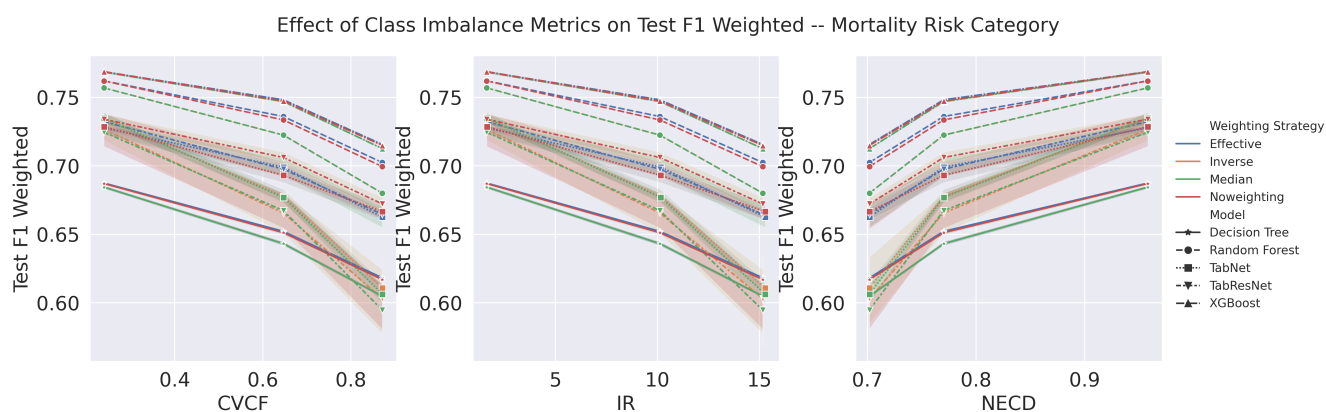


**Figure 15. Class imbalance effect on mortality risk prediction.** Weighted F1 results across model families and reweighting schemes, examined under CVCF, IR, and NECD. Mortality prediction tasks showed marked vulnerability to imbalance, with sharper degradation for neural models (especially TabNet). Tree-based ensembles, and XGBoost in particular, demonstrated comparatively greater resilience. All three metrics captured the same downward trajectory, with NECD declining as imbalance severity increased.

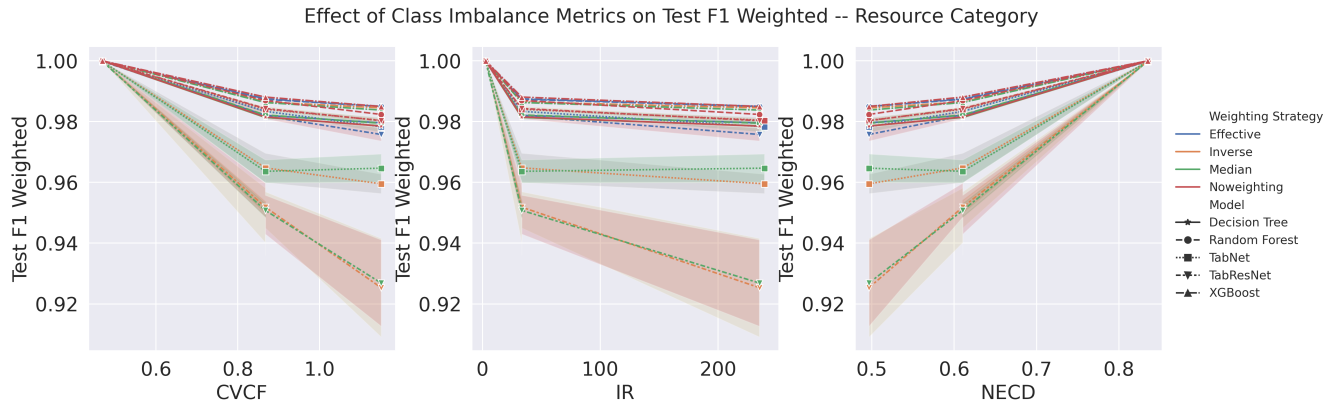


**Figure 16. Influence of imbalance on resource utilization prediction.** Weighted F1 values for five model families (Decision Tree, Random Forest, TabNet, TabResNet, and XGBoost) using four weighting schemes. Results are tracked across three imbalance metrics. While most models experienced only gradual declines in performance, deep learning methods were more susceptible to skew, whereas ensemble methods maintained stronger robustness. CVCF produced slightly more variable curves but remained consistent with IR and NECD, with NECD reliably decreasing as imbalance increased.

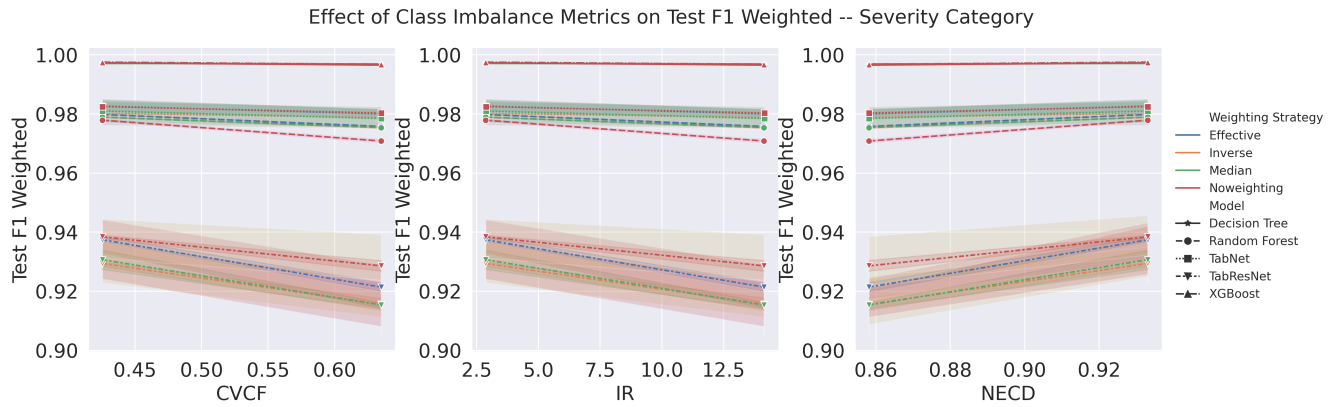


**Figure 17. Performance under class imbalance for severity prediction.** Weighted F1 results comparing all model families and weighting strategies against CVCF, IR, and NECD. Severity classification was less sensitive to imbalance than other tasks, with tree-based ensembles, especially XGBoost, exhibiting stable performance, while neural architectures such as TabNet and TabResNet showed modest but consistent degradation. The three imbalance metrics yielded highly similar performance curves, with NECD monotonically decreasing as imbalance increased.

(fastest training times), followed by TabResNet and Random Forest variants, while TabNet variants consistently had the highest ranks (slowest training times).

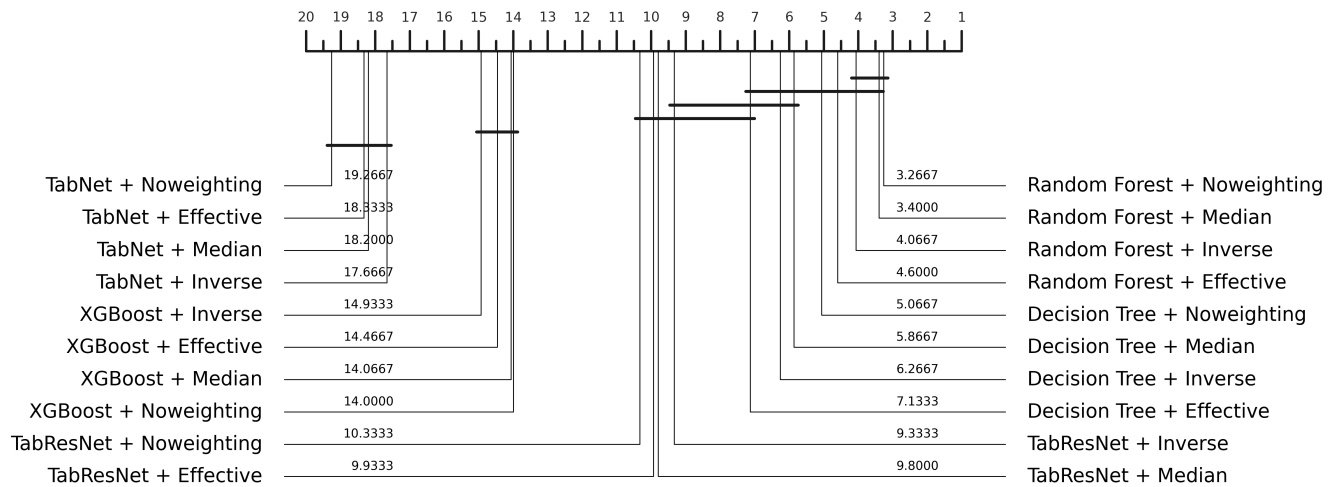


**Figure 18. Critical difference diagram for classifier performance.** Critical difference diagram of the average ranks of 20 classifiers on this dataset, based on weighted F1-scores across experimental blocks. Lower ranks indicate better predictive performance. Horizontal bars connect classifiers that are not significantly different under Wilcoxon signed-rank tests with Holm correction.

### .3.4 Training Time Scaling Plots

Figure 19 presents extended analyses of training time scaling with dataset size across the five prediction tasks in the eICU dataset. Training time is reported on a logarithmic scale and shown for all classifiers and weighting strategies. These plots complement the rank-based comparisons by illustrating absolute training durations and highlighting the scaling gap between tree-based ensembles and deep learning models as sample size increases.

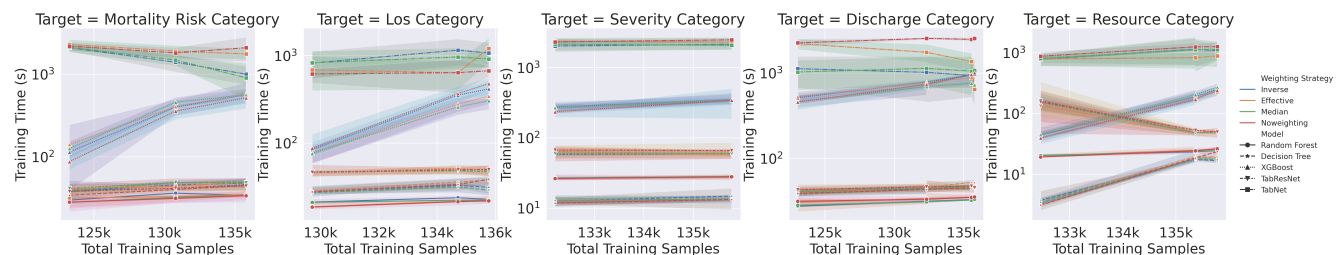


**Figure 19. Training time scaling across prediction tasks.** Training time as a function of dataset size for different prediction tasks. Each panel shows the training time (seconds, log scale) versus the total number of training samples for a specific target variable (mortality risk, length of stay, severity, discharge disposition, and resource utilization). The results are reported across all classifiers and class weighting strategies.

## A Summary of Supplementary Results

The extended results presented here provide additional depth to the main findings. Across both datasets, the supplementary analyses confirmed three consistent trends:

1. Class imbalance metrics (CVCF, IR, and NECD) provide complementary but correlated perspectives on dataset skew. As imbalance increases, IR and CVCF rise, while NECD decreases from 1 toward 0, offering a bounded and interpretable measure of class balance.

2. Tree-based ensembles such as XGBoost maintain superior predictive performance under imbalance compared with deep tabular models.
3. The computational efficiency differences widen as dataset size increases, with simpler models scaling more predictably and deep learning models incurring substantially greater training times.

Together, these extended results reinforce the conclusion that robustness to imbalance and computational scalability are more consequential for deployment in ED and ICU settings than model complexity alone.